Next-to-leading-logarithmic PanScales showers for Deep Inelastic Scattering and Vector Boson Fusion

Melissa van Beekveld,[a] **Silvia Ferrario Ravasio,**[b]

[a]*Rudolf Peierls Centre for Theoretical Physics, Clarendon Laboratory, Parks Road, University of Oxford, Oxford OX1 3PU, UK*

[b]*Theoretical Physics Department, CERN, CH-1211 Geneva 23, Switzerland*

E-mail: melissa.vanbeekveld@physics.ox.ac.uk, silvia.ferrario.ravasio@cern.ch

ABSTRACT: We introduce the first family of parton showers that achieve next-to-leading logarithmic (NLL) accuracy for processes involving a t-channel exchange of a colour-singlet, and embed them in the PanScales framework. These showers are applicable to processes such as deep inelastic scattering (DIS), vector boson fusion (VBF), and vector boson scattering (VBS). We extensively test and verify the NLL accuracy of the new showers at both fixed order and all orders across a wide range of observables. We also introduce a generalisation of the Cambridge-Aachen jet algorithm and formulate new DIS observables that exhibit a simple resummation structure. The NLL showers are compared to a standard transverse-momentum ordered dipole shower, serving as a proxy for the current state-of-the-art leading-logarithmic showers available in public codes. Depending on the observable, we find discrepancies at NLL of the order of 15%. We also present some exploratory phenomenological results for Higgs production in VBF. This work enables, for the first time, to resum simultaneously global and non-global observables for the VBF process at NLL accuracy.

arXiv:2305.08645v3 [hep-ph] 5 Feb 2024

Contents

1 Introduction

Particle-physics collider experiments provide us with a unique opportunity to test our knowledge of the fundamental interactions of elementary particles. Accurately predicting signatures originating from Standard Model (SM) physics is crucial to fully harness the potential of the data, and have sensitivity to possible signals originating from beyond-the-Standard-Model scenarios. Deciphering the nature of the Higgs boson and its interaction with other SM particles is indeed one of the main objectives of the physics programme of the Large Hadron Collider (LHC). General purpose Monte Carlo (GPMC) event generators are fundamental tools in this context. They play a crucial role in our understanding of the phenomenology of colliders, thanks to their ability to describe much of the data from the LHC and its predecessors.

Parton showers lie at the core of GPMCs, and describe the energy degradation of highly-energetic partons that are produced in the hard scattering process, through radiation of soft and/or collinear partons. They enable us to simulate arbitrarily complex collider events, characterised by a large multitude of particles, whose modelling involves physics across a broad range of scales. Despite their fundamental role in collider phenomenology, only in the recent years more attention has been dedicated to understanding and improving the formal accuracy of parton showers. Parton showers resum logarithmic terms in the perturbative series. These terms arise from soft and collinear divergences, and can become large when exploring physics across a wide range of scales. Consequentially, terms of the form $\alpha_s^n \sum_{i=1}^{n+1} c_i L^i$, where L is a large logarithm of a ratio of two disparate scales, will occur at each perturbative order n, with c_i a coefficient that depends on the observable. For example, with the strong coupling $\alpha_s(m_Z) = 0.118$, a hard scale of $m_Z = 91.18$ GeV, and a hadronic scale of $\Lambda = 1$ GeV, the next-to-leading logarithmic (NLL) corrections of the form $\alpha_s \ln(m_Z/\Lambda)$ become of the order of 0.5. This constitutes an $\mathcal{O}(1)$ correction, which needs to be resummed to all orders in the perturbative coupling to obtain an accurate prediction.

The Herwig7 [1, 2] angular-ordered shower, which is based on the coherent branching formalism [3], correctly resums NLL terms (provided a careful interpretation of the ordering variable is performed [4, 5]) for global observables, but not for non-global ones [6]. The NLL terms of the latter cannot be captured by the coherent branching formalism, but require a dipole approach [7], as they are sensitive to the full angular distribution of soft emissions. Another practical advantage of a dipole shower, is that matching with fixed-order matrix elements is much simpler. This has led to numerous techniques to perform multi-jet merging at next-to-leading order (NLO) [8–18] , and matching to fixed-order accuracies, i.e. (next-to-)next-to-next-to-leading order ((N)NNLO) [19–24].[1] Despite the large body of work on improving the fixed-order accuracy of showers, until recently, relatively little has been done on improving their logarithmic accuracy. Indeed, all standard dipole showers currently embedded in public GPMC [28–37] are only leading logarithmic (LL), i.e. they resum terms that are proportional to $\alpha_s^n L^{n+1}$.

---

[1]LO multi-jet merging techniques that can be applied to an angular-ordered showers are discussed in Refs. [25–27].
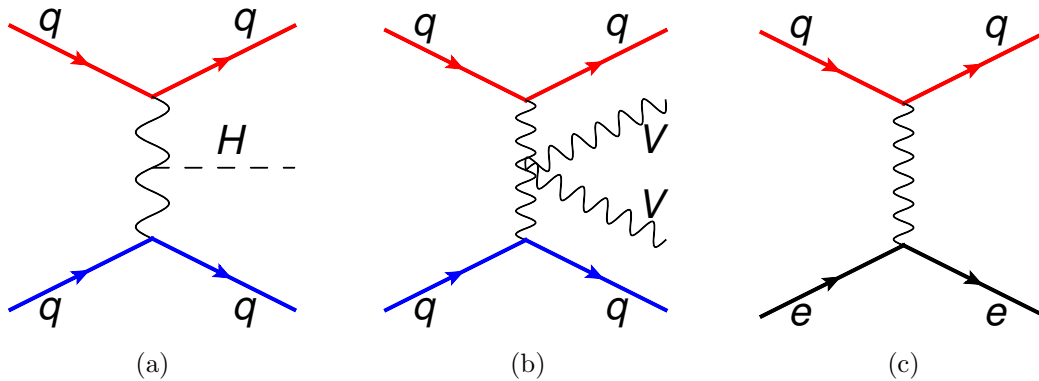
Figure 1: Feynman diagrams contributing to (a) Higgs production in VBF, (b) VBS and (c) DIS. Colour-connected quark lines are highlighted in red and blue. Leptons are represented with black solid lines.

The focus of this paper is to design the first dipole showers for processes characterised by the t-channel exchange of a colour-singlet that reach NLL (here defined to be single-logarithmic, $\alpha_s^n L^n$) accuracy for both global and non-global observables. This work follows on earlier developments of parton showers with a controlled logarithmic accuracy by the PanScales collaboration, like those for dijet production in e^+e^- collisions [38]. Key components in the design of showers is a careful construction of the recoil distribution after a new emission has been generated, and its interplay with the ordering variable of the shower [39]. Several other groups have also been investigating NLL-accurate showers in the context of e^+e^- collisions. Ref. [40] introduced an algorithm that is shown to analytically reproduce NLL accuracy for the thrust distribution and subject multiplicity. The Λ-ordered Deductor shower is shown to be NLL accurate for the thrust distribution in Ref. [41]. Ref. [42] presents Alaric, a shower that is proven to be NLL accurate for a wide range of global observables. Designing NLL showers for hadronic colliders bring additional complications with respect to that for e^+e^- collisions, as the treatment of the recoil from the initial-state is more subtle. In Refs. [43, 44], we presented NLL-accurate dipole showers for the production of a colour singlet at the LHC. At present, no other showers exists with demonstrated NLL accuracy (for both global and non-global observables) for such processes.[2] The present work extends the set of NLL accurate showers to processes characterised by a t-channel exchange of a colour singlet, such that now all processes with at most two partons at the first contributing order can be described at single-logarithmic accuracy for generic observables.

Examples of processes with a t-channel exchange of a colour-singlet, are vector-boson fusion (VBF, Fig. 1a) and vector-boson scattering (VBS, Fig. 1b). Measurements of VBF and VBS processes can provide valuable insight into the electroweak (EW) and Higgs

---

[2]A discussion on the treatment of the transverse-momentum recoil for initial-state radiation in an angular-ordered shower can be found in Ref. [5], as well as in the Herwig++ manual [1]. This topic has also been addressed in Ref. [45] in the context of the transverse-momentum distribution of the Z boson in Drell Yan production, albeit without a claim on the logarithmic accuracy that is achieved.

sectors [46, 47]. Higgs production in VBF is the second most abundant production mode for the Higgs boson at the LHC. It has a clear experimental signature, given by the presence of two back-to-back hard jets in the forward and backward regions of the detectors, and hence it is the preferred channel to for example measure the Higgs coupling to muons [48, 49], tauons [50, 51], and to study Higgs to invisible decays [52, 53]. Run III data will enable us to perform precise determinations of the size of gauge-bosons self-interactions. Modifications to VBS processes are predicted in models of physics beyond the SM, through changes to the Higgs boson couplings to gauge bosons and the resonant production of new particles. Differences in the parton-shower modelling turn out to be one of the leading uncertainty in these kind of processes [49–51, 54–62]. Having access to several NLL-accurate showers, such as the ones we present in this article, will help to assess more realistic shower uncertainties, and possibly reduce them.

Higher-order QCD contributions to VBF and VBS processes are computed using a factorised approach [63–65], i.e. neglecting non-factorisable corrections stemming from the exchange of partons between the two hadronic sectors, which are coloured in red and blue in Figs. 1a and 1b. Non-factorisable corrections appear only from NNLO and are typically colour-suppressed with respect to the factorisable ones [66, 67]. In the factorised approximation, radiative corrections to VBF and VBS are closely related to those for deep inelastic scattering (DIS, Fig. 1c).[3] For this reason, the first part of this article focuses on the formulation of the PanScales showers for DIS processes. We then extend our showers to handle two copies of DIS, so that they can also be used to describe VBF and VBS events in the factorised approach. After including mass effects, which we leave for future work, this framework will also enable us to handle t-channel single-top production. These showers will have full colour accuracy at LL, and leading colour accuracy at NLL, i.e. single-logarithmic in our definition. This is the first time this logarithmic accuracy is reached, either analytically or numerically, for the VBF and VBS processes.

In addition to its relevance to hadron-collider processes involving a colourless t-channel exchange, an improved theoretical framework for deep inelastic scattering (DIS) can be directly applied to interpret data gathered from electron-proton (ep) colliders like the Hadron Electron Ring Accelerator (HERA). These colliders provide an ideal environment for investigating the internal structure of hadrons and conducting accurate studies of quantum chromodynamics (QCD). The new-generation of lepton-hadron colliders, such as the Electron-Ion Collider (EIC), whose construction is planned to start next year, would also

---

[3]VBF can be treated using the structure function approach, i.e. treating the two quark lines as two seperate copies of DIS. Instead, for VBS, interferences between diagrams with a t-channel exchange of a boson and the tagged bosons being emitted from the quark legs directly spoil this picture. From the QCD point of view, one can still use the factorised approximation and neglect gluon exchanges between the two quark lines, also see Ref. [47] and references therein. However, for the VBS topology, one needs to decide whether a boson needs to be boosted together with all partons belonging to one hadronic sector, to preserve its angle with respect to the original-final state quark, which is sensible when that boson was emitted directly from the quark line. Otherwise, the shower may reshuffle the post-branching momenta in such a way that the boson becomes collinear to the jet, or that a collinear boson is suddenly emitted at a wide angle: in both situations, the matrix element used to generate the process would then no longer describe the post-branching situation with the new four-momenta.

benefit from more accurate MC generators.

The paper is structured as follows. In Sec. 2 we review the standard kinematic variables used in DIS. In Sec. 3 we present the common building-blocks of a generic dipole-shower for DIS. In Sec. 3.1, we summarise the main features of a standard dipole shower, while in Sec. 3.2 we present the new PanScales showers for DIS, whose extension to VBF/VBS is discussed in Sec. 3.3. We then perform fixed-order tests of such showers in Sec. 4. The all-orders validations of the PanScales showers are instead performed in Sec. 5. We test numerous observables, designed to probe soft and/or collinear emissions that an NLL shower should accurately describe: the DGLAP evolution of the parton distribution functions (Sec. 5.1), average particle multiplicity (Sec. 5.2), several continuously-global observables (Sec. 5.3), and the amount of radiation in a rapidity slice (Sec. 5.4), which we consider as a proxy for a generic non-global observable. In Sec. 6 we show some phenomenological results for Higgs production in VBF, and in Sec. 7 we present our conclusions.

2 DIS definition and kinematics

We consider the DIS process $\gamma^* p \to X$, where p is the incoming proton, γ^* is a space-like photon (or more generically a colourless boson) and X is a generic hadronic final-state. We denote with q_{DIS}^μ the photon momentum, and we define

$$Q^2 = -q_{\mathrm{DIS}}^2 > 0 \,. \tag{2.1}$$

The (massless) proton momentum is denoted by P^μ. We introduce two light-like reference vectors n_1 and n_2, such that n_1 is parallel to the incoming proton i.e.

$$n_1^\mu = x_{\mathrm{DIS}} P^\mu \,, \tag{2.2}$$

and

$$n_2^\mu = q_{\mathrm{DIS}}^\mu + n_1^\mu \,. \tag{2.3}$$

Requiring that $n_2^2 = 0$ leads to

$$x_{\mathrm{DIS}} = \frac{Q^2}{2 \, q_{\mathrm{DIS}} \cdot P} \,. \tag{2.4}$$

Furthermore, we see that $n_1 \cdot n_2 = Q^2/2$. At the partonic level, the lowest-order contribution reads $\gamma^* q \to q$, where the incoming (outgoing) quark momentum is precisely n_1^μ (n_2^μ). More generally, if the sum of the momenta of the final-state partons has an invariant mass M_X, one may always parameterise their collective momentum p_X^μ as

$$p_X^\mu = n_2^\mu + \frac{M_X^2}{Q^2} n_1^\mu \,. \tag{2.5}$$

Momentum conservation then implies that the incoming parton has momentum

$$p_1^\mu = \left(1 + \frac{M_X^2}{Q^2}\right) n_1^\mu = x_1 P^\mu, \quad \text{with} \quad x_1 = x_{\mathrm{DIS}} \left(1 + \frac{M_X^2}{Q^2}\right). \tag{2.6}$$

Indeed, with these definitions we have

$$p_1^\mu + q_{\text{dis}}^\mu = p_X^\mu \,. \tag{2.7}$$

We work in the Breit frame [68], which is defined as the frame where n_1 and n_2 are back-to-back and aligned along the z-axis, i.e.

$$n_1^\mu = \frac{Q}{2}\,(0,0,-1;1)\,, \qquad n_2^\mu = \frac{Q}{2}\,(0,0,+1;1)\,, \tag{2.8a}$$

$$q_{\text{DIS}}^\mu = Q\,(0,0,+1;0)\,, \tag{2.8b}$$

with $Q \equiv \sqrt{Q^2}$. The final-state momenta can then always be decomposed in terms of Sudakov variables, i.e.

$$k_i^\mu = \alpha_i n_1^\mu + \beta_i n_2^\mu + k_{\perp i}^\mu \,, \tag{2.9}$$

where $k_{\perp i}^\mu$ is a generic space-like vector orthogonal to $n_{1,2}^\mu$. Partons are said to reside in the current hemisphere when $\beta_i > \alpha_i$. The remnant hemisphere instead contains partons with $\alpha_i > \beta_i$. When constructing the shower, it will turn out to be convenient to introduce the reference vector

$$Q^\mu = n_1^\mu + n_2^\mu \,, \tag{2.10}$$

which has norm $Q^2 = -q_{\text{DIS}}^2$. We note that the energy component in the Breit frame of a given momentum p^μ is obtained through

$$E_{\text{Breit}} = \frac{p \cdot Q}{Q} \,. \tag{2.11}$$

We will use the reference vector Q^μ in the formulation of the PanScales showers to measure angular distances in the Breit frame instead of the dipole frame.

3 Dipole showers for DIS and VBF/VBS

The fundamental building block for a dipole shower is a $2 \to 3$ branching kernel [7]. In these types of showers each emitter $\tilde{\imath}$ is colour-connected (understood in the limit of a large number of colours N_{C}) to a spectator $\tilde{\jmath}$, such that the branching is $\tilde{\imath}\tilde{\jmath} \to ijk$, with k the radiated parton. Dipole showers for DIS (and VBF or VBS) need to handle emissions that come from dipoles that contain two final-state partons (FF dipoles), or one parton in the initial state and one in the final state (IF dipoles).

First, we consider an FF dipole with pre-splitting momenta $\tilde{p}_i$, $\tilde{p}_j$, and post-splitting momenta p_i, p_j, p_k. The momentum of the radiated parton k may be decomposed as

$$p_k^\mu = z_i \tilde{p}_i^\mu + z_j \tilde{p}_j^\mu + k_\perp^\mu \,. \tag{3.1}$$

where $k_\perp^\mu$ is a space-like vector orthogonal to $\tilde{p}_{i,j}^\mu$. In this notation with $\tilde{p}_i$ identified as emitter, z_i corresponds to the collinear momentum fraction carried away by the emission p_k, defined relative to the pre-branching momentum. The emission probability that describes correctly radiation in the soft and collinear limit can be written as

$$\mathrm{d}\mathcal{P}_{\tilde{\imath}\tilde{\jmath}\to ijk} = \frac{\alpha_s(\mu_{\mathrm{R}}^2)}{2\pi}\left(1 + \frac{\alpha_s(\mu_{\mathrm{R}}^2)K}{2\pi}\right)\frac{\mathrm{d}v^2}{v^2}\mathrm{d}\bar{\eta}\frac{\mathrm{d}\phi}{2\pi}\left[g(\bar{\eta})z_i P_{ik}^{\mathrm{FS}}(z_i) + g(-\bar{\eta})z_j P_{jk}^{\mathrm{FS}}(z_j)\right], \quad (3.2)$$

where μ_{R}^2 is the renormalisation scale. The phase space of the emission is parameterised by the shower variables v and $\bar{\eta}$, where v can be identified with the shower ordering scale, and $\bar{\eta}$ is a rapidity-like auxiliary variable. The exact relation between $z_i, (z_j), k_\perp$ and the shower variables $v, \bar{\eta}$ is shower dependent and will be detailed in the following sections. The azimuthal angle of the radiation defined with respect to the plane spanned by the two pre-branching dipole momenta is denoted by ϕ. To achieve NLL accuracy one needs to evaluate the running of the coupling at two loops, with μ_{R} equal to the transverse-momentum of the emission in the soft-collinear limit. In addition, the soft-collinear gluon emission probability must include an $\alpha_s K/(2\pi)$ correction term with $K = (67/18 - \pi^2/6)C_A - 5n_f/9$ [69]. We take $C_A = 3$, $T_R = 1/2$ and we work with $n_f = 5$ light flavours (unless otherwise stated). The definition of the DGLAP final-state splitting functions $P^{\mathrm{FS}}(z)$ that we use is given in appendix A of Ref. [43], with their soft limit obtained as $z \to 0$. Following Ref. [38], we use two definitions of g:

$$g(\bar{\eta}) = g^{\mathrm{dip.}}(\bar{\eta}) \equiv \begin{cases} 0 & \text{if } \bar{\eta} < -1, \\ \frac{15}{16}\left(\frac{\bar{\eta}^5}{5} - \frac{2\bar{\eta}^3}{3} + \bar{\eta} + \frac{8}{15}\right) & \text{if } -1 < \bar{\eta} < 1, \\ 1 & \text{if } \bar{\eta} > 1, \end{cases} \quad (3.3)$$

or

$$g(\bar{\eta}) = g^{\mathrm{ant.}}(\bar{\eta}) \equiv \frac{e^{\bar{\eta}}}{e^{\bar{\eta}} + e^{-\bar{\eta}}} = \frac{e^{2\bar{\eta}}}{e^{2\bar{\eta}} + 1}. \quad (3.4)$$

We use $g^{\mathrm{ant.}}$ for antenna showers, where one makes no distinction between an emitter/spectator to distribute the transverse-momentum recoil, while we use $g^{\mathrm{dip.}}$ when only one of the parent partons takes the transverse recoil.

Instead, for IF dipoles where we define the parton $\tilde{\imath}$ as belonging to the initial-state, we write the momentum of the radiated parton as

$$p_k^\mu = \frac{z_i}{1 - z_i}\tilde{p}_i^\mu + z_j\tilde{p}_j^\mu + k_\perp^\mu. \quad (3.5)$$

The emission probability then takes the form

$$\mathrm{d}\mathcal{P}_{\tilde{\imath}\tilde{\jmath}\to ijk} = \frac{\alpha_s(\mu_{\mathrm{R}}^2)}{2\pi}\left(1 + \frac{\alpha_s(\mu_{\mathrm{R}}^2)K}{2\pi}\right)\frac{\mathrm{d}v^2}{v^2}\mathrm{d}\bar{\eta}\frac{\mathrm{d}\phi}{2\pi}$$
$$\times\left[\frac{x_i f_i(x_i, \mu_{\mathrm{F}}^2)}{\tilde{x}_i f_{\tilde{\imath}}(\tilde{x}_i, \mu_{\mathrm{F}}^2)}g(\bar{\eta})z_i P_{ik}^{\mathrm{IS}}(z_i) + g(-\bar{\eta})z_j P_{jk}^{\mathrm{FS}}(z_j)\right], \quad (3.6)$$

where f_i is the PDF of the incoming parton i, and $x_i = \frac{\tilde{x}_i}{1 - z_i}$. The choice of the factorisation scale μ_{F} depends on the ordering variable v, and it must be chosen such that for a hard-collinear initial-state branching, μ_{F} is equal to the transverse momentum of the emission. The definition of the DGLAP initial-state splitting functions is also given in Appendix A of Ref. [43].

The DIS invariants q^2_{DIS} and x_{DIS}, introduced in the previous section, determine the structure of the event. At LO these two invariants are the only two quantities needed to describe the interaction between the incoming lepton and nucleon. Although unitarity of the shower is preserved, the real-virtual cancelation on more differential LO observables is spoiled when modifying the DIS invariants through the generation of an emission. Preserving the LO DIS invariants is therefore crucial to ensure that the shower does not alter the description of any inclusive observable. Furthermore, this also simplifies the inclusion of higher-order corrections in future works, especially in the context of VBF if the two hadronic sectors evolve completely independently. For these reasons, the conservation of the DIS invariants q^2_{DIS} and x_{DIS} is a fundamental property of all the showers we consider/develop here.

3.1 A standard transverse-momentum-ordered dipole shower

In this section, we briefly summarise the fundamental features of a standard dipole shower, which we use as a proxy to illustrate the behaviour of current standard leading-logarithmic showers that are used for DIS and VBF/VBS phenomenological studies. It is based on a Catani-Seymour dipole-local map, as first explored in Refs. [7, 70]. We refer to this shower as "Dipole-k_t", and its kinematic maps (with local momentum conservation in the IF and FF dipoles) are presented in Refs. [43, 44].[4] All publicly-available dipole showers for DIS collisions, such as Pythia8 with dipole-local recoil [31], Sherpa [28], and Herwig's dipole shower [29] share a great degree of similarity with Dipole-k_t in the small transverse-momentum limit. Differences can be large away from the small transverse-momentum limit. However, the degrees-of-freedom relevant for logarithmic accuracy, as shown in [39], namely the frame in which the emitter and spectator are chosen (the dipole centre-of-mass frame), the ordering variable of the shower (transverse-momentum ordered), and the transverse-momentum recoil scheme, are the same for the showers mentioned above.[5] Here we review the basic characteristics of the Dipole-k_t shower.

The ordering variable v of the Dipole-k_t shower algorithm is transverse-momentum-like, i.e. it corresponds to the transverse momentum of the emitted particle in the limit that this emission is soft-collinear. The rapidity-like variable $\bar{\eta}$, used to partition the dipole in two halves, can be related to the collinear momentum fraction z. This relation reads

$$\bar{\eta} = \begin{cases} \frac{1}{2} \ln \frac{z^2 \tilde{s}_{ij}}{v^2} & \text{(final state)}, \\ \frac{1}{2} \ln \frac{z^2 \tilde{s}_{ij}}{(1-z)^2 v^2} & \text{(initial state)}, \end{cases} \tag{3.7}$$

with $\tilde{s}_{ij} = 2\tilde{p}_i \cdot \tilde{p}_j$ the dipole invariant mass. From this it is clear that $\bar{\eta}$ partitions the dipole in its rest frame. In the Dipole-k_t shower, momentum conservation is fully local. This implies that when an emission occurs from a FF dipole, the transverse momentum recoil is entirely taken up by the emitter, which corresponds to the original dipole leg closer in angle to the emission. Conversely, in an IF dipole, the transverse momentum recoil is

---

[4]In particular, the kinematic maps coincide with those of the Dire-v1 shower [30].

[5]Albeit an antenna shower, this also makes us believe that Vincia [71] has the same logarithmic order of accuracy as Dipole-k_t.

always absorbed by the final-state leg. The factorisation and renormalisation scales are set equal to v. Further details on the kinematic maps used in the Dipole-k_t shower are given in Appendix B.1 of Ref. [43].[6]

3.2 PanScales showers for DIS

The PanScales showers need a reference momentum Q^μ to define a common frame where to measure angular distances for all the emissions, which here we take to be the Breit frame. We set this equal to Q^μ as introduced in eq. (2.10), which in the Breit frame reads $Q^\mu = (0, 0, 0; Q)$. The ordering variable v is defined in such a way that for a soft-collinear emission of transverse momentum $k_\perp$ and rapidity η, we have

$$v \approx k_\perp e^{-\beta_{\mathrm{PS}}|\eta|} \,. \tag{3.8}$$

We also introduce the shower variable $\bar{\eta}_Q$, that corresponds to the rapidity of a soft-collinear emission in the Breit frame. Given the shower variables v and $\bar{\eta}_Q$, we can define a transverse-momentum auxiliary variable

$$\kappa_\perp \equiv \rho v e^{\beta_{\mathrm{PS}}|\bar{\eta}_Q|} \,, \tag{3.9}$$

where we have used

$$\tilde{s}_i = 2\tilde{p}_i \cdot Q \,, \quad \tilde{s}_j = 2\tilde{p}_j \cdot Q \,, \quad \tilde{s}_{ij} = 2\tilde{p}_i \cdot \tilde{p}_i \,, \quad \rho = \left(\frac{\tilde{s}_i \tilde{s}_j}{\tilde{s}_{ij} Q^2} \right)^{\beta_{\mathrm{PS}}/2} \,. \tag{3.10}$$

To achieve NLL accuracy, the renormalisation scale at which the coupling constant is evaluated is set to $\kappa_\perp$, while for the factorisation scale we choose

$$\mu_{\mathrm{F}} = Q \left(\frac{v}{Q} \right)^{\frac{1}{1+\beta_{\mathrm{PS}}}} \,. \tag{3.11}$$

We also introduce the variables

$$\alpha_k \equiv \sqrt{\frac{\tilde{s}_i}{\tilde{s}_j \tilde{s}_{ij}}} \kappa_\perp e^{\bar{\eta}_Q} \,, \qquad \beta_k \equiv \sqrt{\frac{\tilde{s}_j}{\tilde{s}_i \tilde{s}_{ij}}} \kappa_\perp e^{-\bar{\eta}_Q} \,, \tag{3.12}$$

which enable us to write the light-cone momentum fraction at which we need to evaluate the DGLAP splitting probabilities appearing in eqs. (3.2), (3.6). If the original-dipole legs $\tilde{\imath}$ and $\tilde{\jmath}$ are final-state partons, we define

$$z_i = \alpha_k \,, \qquad z_j = \beta_k \,, \tag{3.13}$$

while if $\tilde{\imath}$ is an incoming parton, the definition of z_i is modified and we instead use

$$z_i = \frac{\alpha_k}{1 - \alpha_k} \,. \tag{3.14}$$

---

[6]Conversely to Refs. [43, 44], here we use only the local variant of Dipole-k_t and we do not consider the global variant. The latter algorithm does not preserve the DIS invariants (specifically x_{DIS} and $y_{\mathrm{DIS}} = \frac{Q^2}{x_{\mathrm{DIS}} s}$) and for this reason it has never been used in phenomenological applications to DIS or VBF/VBS.

3.2.1 PanGlobal

This section details the kinematic mapping of an antenna shower with global transverse-momentum recoil. We refer to this shower as PanGlobal. The treatment of the longitudinal recoil is similar to the proposal for the PanGlobal variant for hadron collisions of Refs. [43, 44]. The main difference is represented by the boost that is performed to achieve momentum conservation in the perpendicular component. This choice is motivated by the fact that in our case we want to preserve q_{DIS}^{μ}, i.e. the momentum of the t-channel exchanged boson, while for colour-singlet production the most natural variables to preserve are the invariant mass and the rapidity of the colour singlet system. One begins by introducing some intermediate post-branching dipole momenta, which read

$$\bar{p}_i^{\mu} = r_{\mathrm{L}}(1 \pm a_k)\tilde{p}_i^{\mu} \,, \tag{3.15a}$$

$$\bar{p}_j^{\mu} = r_{\mathrm{L}}(1 \pm b_k)\tilde{p}_j^{\mu} \,, \tag{3.15b}$$

$$\bar{p}_k^{\mu} = r_{\mathrm{L}}(a_k\tilde{p}_i^{\mu} + b_k\tilde{p}_k^{\mu} + k_{\perp}^{\mu}) \,, \tag{3.15c}$$

with $a_k = \alpha_k$, $b_k = \beta_k$ and

$$k_{\perp}^{\mu} = \sqrt{a_k b_k \tilde{s}_{ij}} \left(\hat{k}_{\perp 1}^{\mu} \sin\phi + \hat{k}_{\perp 2}^{\mu} \cos\phi \right) , \tag{3.16}$$

with $\hat{k}_{\perp 1,2}$ two vectors with norm -1 orthogonal to $\tilde{p}_{i,j}$ such that $\hat{k}_{\perp 1} \cdot \hat{k}_{\perp 2} = 0$. The signs in eq. (3.15) depend on whether the $\tilde{\imath}$ or $\tilde{\jmath}$ is incoming $(+)$ or outgoing $(-)$. The momentum mapping of eq. (3.15) clearly does not conserve momentum. Indeed we have

$$\bar{p}_X^{\mu} - \bar{p}_1^{\mu} = q_{\mathrm{dis}}^{\mu} + r_{\mathrm{L}}k_{\perp}^{\mu} + (r_{\mathrm{L}} - 1)(\tilde{p}_j^{\mu} \pm \tilde{p}_i^{\mu}) \,. \tag{3.17}$$

where we have the $-$ sign for $i = 1$ (an IF dipole) and $+$ otherwise (FF dipoles), and $\bar{p}_X$ is the sum of the momenta of all the post-branching final-state partons. At variance with the original proposal Refs. [43, 44], we have introduced a local rescaling factor r_{L}, whose value depends on the type of the dipole. In particular, we have

$$r_{\mathrm{L}} = \begin{cases} \dfrac{\tilde{s}_i + \tilde{s}_j}{\tilde{s}_i + \tilde{s}_j + 2k_{\perp} \cdot Q} & \text{FF dipoles} \\ 1 & \text{IF dipoles.} \end{cases} \tag{3.18}$$

As explained in Appendix B and in Ref. [72], the local rescaling factors r_{L} ensure that triple-collinear FF configurations (where k_t^2 is small, but $k_{\perp} \cdot Q$ can potentially be large) do not result in a large boost, or a large rescaling for $\tilde{p}_1$ in Eq. (3.20) below. The form of r_{L} originates from imposing $\tilde{p}_X \cdot Q = \bar{p}_X \cdot Q$, which acts as to preserve the energy of final state before and after the emission. As further detailed in Appendix B, no such factor is necessary for IF dipoles, hence we set $r_{\mathrm{L}} = 1$. We stress that for small values of $2k_{\perp} \cdot Q$, i.e. when either a_k or b_k are small, we have $r_{\mathrm{L}} = 1$.

There is a considerable amount of freedom in how to implement the momentum reshuffling to restore momentum conservation. However, at NLL accuracy, it is important to ensure that partons in the remnant hemisphere are only marginally affected by the recoil from emissions widely separated in angle. For instance, one could choose to only boost the

partons in the current hemisphere. However, we can find a configuration where the current hemipshere is populated by only soft wide-angle emissions. Constructing the boost such that all the recoil is given to soft partons would then lead to infrared unsafe results. [73]. For this reason, we devised a smooth Lorentz transformation that acts on all partons, but primarily modifies those with a substantial component along n_2^μ. First, we first adjust the momentum of the incoming parton p_1^μ so that

$$(p_1 + q_{\text{dis}})^2 = \bar{p}_X^2. \tag{3.19}$$

Requiring that p_1^μ only has a component in the direction of n_1^μ, gives us

$$p_1^\mu = \left(1 + \frac{\bar{p}_X^2}{Q^2}\right) n_1^\mu = \left(\frac{Q^2 + \bar{p}_X^2}{Q^2 + \tilde{p}_X^2}\right) \tilde{p}_1^\mu, \tag{3.20}$$

where $\tilde{p}_X^\mu = \tilde{p}_1^\mu + q_{\text{DIS}}^\mu$ denotes the pre-branching partonic final-state. Finally, we boost the post-branching partonic final-state momenta from $\bar{p}_X^\mu$ to

$$p_X^\mu = n_2^\mu + \frac{\bar{p}_X^2}{Q^2} n_1^\mu. \tag{3.21}$$

The boost is constructed to ensure that partons parallel to the incoming proton do not acquire any transverse-momentum. Instead, this component is absorbed by partons carrying a substantial fraction of the original final-state quark momentum n_2^μ. The boost that achieves this is derived in Appendix A and reads

$$\Lambda^{\mu\nu} = g^{\mu\nu} + \frac{2n_1^\mu}{Q^2} \left[(\beta - 1)n_2^\nu + \frac{p_t^2}{\beta Q^2} n_1^\nu + p_\perp^\nu\right] + \frac{2n_2^\mu n_1^\nu}{Q^2} \frac{1 - \beta}{\beta} - \frac{2p_\perp^\mu n_1^\nu}{\beta Q^2}. \tag{3.22}$$

The components β and $p_\perp$ are defined through a Sudakov decomposition of the final-state momentum sum

$$\bar{p}_X^\mu = \frac{\bar{p}_X^2 + p_t^2}{\beta Q^2} n_1^\mu + \beta n_2^\mu + p_\perp^\mu, \tag{3.23}$$

with $p_\perp$ a space-like vector orthogonal to n_1^μ, n_2^μ with norm $-p_t^2$. Notice that for a_k and/or b_k very small, we have $1 - \beta \sim p_t \sim \kappa_t$, so the boost minimally alter the final-state momenta. Similarly, when a_k or b_k are small, for FF emissions we have that $p_1 \approx \bar{p}_1$, so also the additional rescaling we apply to the incoming parton.

3.2.2 PanLocal

In this section, we describe how to implement a dipole shower with local recoil for DIS, which we refer to as PanLocal.[7] For all three dipole types (IF, FI and FF), we parameterise the momentum of the radiated parton as

$$\bar{p}_k^\mu = a_k \tilde{p}_i^\mu + b_k \tilde{p}_k^\mu + k_\perp^\mu. \tag{3.24}$$

---

[7]We omit the description of an antenna PanLocal version, as future applications such as NLO matching or multi-jet merging would be substantially more cumbersome, as found in Ref. [74].

The emitter can either be an initial-state parton (for IF dipoles), or a final-state one (for FI and FF dipoles). In the former case we use

$$a_k = \alpha_k, \qquad b_k = \beta_k(1 + \alpha_k)^{\frac{2}{1+\beta_{\mathrm{PS}}}}. \tag{3.25}$$

This choice was introduced in Ref. [43] to restore transverse-momentum ordering for very hard-collinear emissions, and serves to avoid unphysical correlations between emissions in opposite hemispheres. Like in Refs. [43, 44], the new momenta of the emitter and the spectator become

$$\bar{p}_i^\mu = (1 + a_k)\tilde{p}_i^\mu + \frac{a_k b_k}{1 + a_k}\tilde{p}_j^\mu + k_\perp^\mu, \tag{3.26}$$

$$\bar{p}_j^\mu = \left(1 - \frac{b_k}{1 + a_k}\right)\tilde{p}_j^\mu. \tag{3.27}$$

Although the momentum is locally conserved (i.e. $\bar{p}_X^\mu - \bar{p}_1^\mu = q_{\mathrm{DIS}}^\mu$), we now end up in a situation where the incoming parton is no longer aligned with the beam direction n_1^μ. The Lorentz transformation that we apply to realign the incoming parton with the beam differs from the one applied for colour-singlet production, since in this case we want to preserve the DIS invariants. After this transformation, the momentum of the incoming parton becomes

$$p_i^\mu = p_1^\mu = \left(1 + \frac{\bar{p}_X^2}{Q^2}\right)n_1^\mu, \tag{3.28}$$

and the sum of final-state partons

$$p_X^\mu = n_2^\mu + \frac{\bar{p}_X^2}{Q^2}n_1^\mu. \tag{3.29}$$

To achieve this, we first rotate all momenta except the photon momentum q_{dis}^μ with a rotation matrix $R(\theta)$. This matrix is defined to align the post-branching incoming parton momentum $\bar{p}_1$ along the direction of n_1^μ. This operation introduces a momentum imbalance since we do not change the photon momentum q_{dis}^μ. To restore momentum conservation we proceed in the same way as for PanGlobal, i.e. we Sudakov decompose the sum of (rotated) final-state momenta as

$$(R(\theta) \cdot \bar{p}_X)^\mu = \frac{\bar{p}_X^2 + p_t^2}{\beta Q^2}n_1^\mu + \beta n_2^\mu + p_\perp^\mu, \tag{3.30}$$

and apply the boost of eq. (3.22) to all partons including the initial-state one.

In the case where the emitter is instead a final-state parton we set

$$a_k = \alpha_k, \qquad b_k = \beta_k. \tag{3.31}$$

The momenta of the emitter and spectator in the case of an FF/FI dipole reads

$$\bar{p}_i^\mu = (1 - a_k)\tilde{p}_i^\mu + \frac{a_k b_k}{1 - a_k}\tilde{p}_j^\mu - k_\perp^\mu, \tag{3.32}$$

$$\bar{p}_j^\mu = \left(1 \pm \frac{b_k}{1 - a_k}\right)\tilde{p}_j^\mu, \tag{3.33}$$

where the $+(-)$ sign is required for FI(FF) dipoles. Note that no boost/rotation needs to be performed in these cases since the initial-state parton does not acquire a transverse momentum component. Hence, $\bar{p}^{\mu}_{i,j,k} = p^{\mu}_{i,j,k}$ for FI and FF dipoles.

3.3 Extension to VBF and VBS

From the point of view of QCD radiative corrections, VBF (Fig. 1a) and VBS (Fig. 1b) can be seen as a double copy of DIS (Fig. 1c). Non-factorisable corrections arising from the exchange of partons between the two hadronic sectors are colour suppressed and only contribute from order α_s^2. They were computed for the first time in Ref. [66] for Higgs production in VBF, using the eikonal approximation, and found to be typically ten times smaller than the NNLO factorisable corrections [75–77], as confirmed by the phenomenological study of Ref. [67], which also addresses double Higgs production.

For this reason, to shower a VBF or VBS process, we treat the two hadronic sectors as two separate and independent DIS processes. This is done by labelling the two sectors a and b, and using for each of them a separate reference vector Q_a^{μ} and Q_b^{μ} that reads

$$Q_a^{\mu} = n_{1,a}^{\mu} + n_{2,a}^{\mu}, \tag{3.34}$$

where $n_{1,a}^{\mu}, n_{2,a}^{\mu}$ are the light-like reference vectors introduced in Sec. 2 such that $q^{\mu}_{\text{DIS,a}} = n_{2,a}^{\mu} - n_{1,a}^{\mu}$. Here $q^{\mu}_{\text{DIS,a}}$ describes the four-momentum of the t-channel colour-singlet boson that is exchanged between the initial- and final-state partons. A similar definition is employed for sector b, with different light-like reference vectors $n_{1,b}^{\mu}$ and $n_{2,b}^{\mu}$. Since the showering of the two hadronic sectors is completely factorised, we have the freedom to choose different values for the shower starting scale for the two different sectors, as well as the factorisation and renormalisation scales employed in the underlying fixed-order calculation.

Once we have established SL accuracy for the showers in the DIS process, extending this accuracy to VBF topologies is conceptually straightforward (especially in the case of VBF), with the exception of non-factorisable corrections, which are not included.[8] The terms that we are neglecting are colour-suppressed NLL corrections. Describing correctly the factorisable contributions is however sufficient to obtain full-colour accuracy at LL, and NLL accuracy in the large N_{C} limit. Additionally, non-factorisable contributions are typically suppressed after applying VBF cuts [67], and also unknown in their complete form (only approximated results have been obtained at fixed order in Ref. [66]).

4 Fixed-order tests

One fundamental property that NLL-accurate parton showers must satisfy is that emissions widely separated in rapidity or transverse momentum must be independent [39]. This

---

[8]We remind the reader that interferences between the diagrams where the tagged bosons in the VBS process are connected to the t-channel propagator (Fig. 1b), and those where the tagged bosons in the VBS process are emitted directly from the quark legs spoil the structure-function picture, so higher-order corrections to the VBS process are not simply those for DIS squared.

requirement follows from the factorisation properties of the underlying QCD matrix element in the limit of soft and/or collinear emissions. It can be directly translated into a "fixed-order" criterion: "a soft emission can alter the momentum of a previously radiated parton only if they are very close in rapidity and emitted with a commensurate transverse momentum".

To better understand this requirement, consider an emission with momentum $\tilde{k}_1^\mu$ from a dipole. After this, the shower will try to generate a second emission, with momentum k_2^μ. The redistribution of momenta (either directly in the kinematic map or via a momentum-conserving boost) may alter the kinematics of the first emission, i.e. $\tilde{k}_1^\mu \to k_1^\mu$. The result is that the event now has two emissions with momenta k_1^μ and k_2^μ, but the first emission was generated with a matrix element corresponding to $\tilde{k}_1^\mu$. The matrix element corresponding to k_1^μ and $\tilde{k}_1^\mu$ are not the same when these momenta are vastly different, hence this would destroy the factorisation property it must obey when k_2^μ is either collinear to any of the partons in the pre-branching event or very soft. This process gets repeated for every emission that follows, leading to a wrong logarithmic exponentiation starting at NLL (at leading colour accuracy). To verify the condition above, in Sec. 4.1 we investigate the behaviour of the showers introduced in the previous section in the presence of two gluons emitted at commensurate values of the ordering variable v.[9]

Another fixed-order criterion that we test is that subleading-colour corrections are correctly implemented in case of strongly-ordered emissions. Indeed, dipole showers are implemented in the large-N_{C} limit, but subleading (i.e. $\propto 1/N_{\mathrm{C}}^2$) corrections in the LL contribution have the same numerical size of NLL terms, thus from a phenomenological point of view they have the same relevance and must be included. For this reason, in Sec. 4.2 we considered two strongly-ordered emissions and we assess whether subleading-colour corrections have been correctly incorporated in the shower at fixed order through a comparison to the exact analytic matrix element. Note that this algorithm is expected to not only yield the correct result at LL full-colour, but also at NLL for many observables, such as average particle multiplicity (Sec. 5.2) and global observables (Sec. 5.3), as well as for the DGLAP evolution (Sec. 5.1).

The final ingredient necessary to reach NLL is the implementation of spin correlations to correctly reproduce the azimuthal distributions of the radiation. To this aim, in appendix F we show that the algorithm introduced in Ref. [43] for PanScales showers for hadron collisions can be applied also to DIS-type processes. However, since spin correlations do not impact the NLL resummation of the observables we use to validate the NLL accuracy of our showers at all orders (detailed in Sec. 5), we do not include them in our all-order tests.

_____

[9]Note that this is a necessary, but not sufficient requirement to reach NLL accuracy for global observables. For the latter, it is important that any pair of emissions are described accurately in the shower, while in the fixed-order test of Sec. 4.1 only the action of the second emission on the first emission's momentum is probed.

4.1 Lund-plane contours

In this section, we investigate if emissions of commensurate hardness are independent when widely separated in angle, as required to achieve NLL accuracy. We consider the DIS process $q\gamma^* \to q$, with $x_{\mathrm{DIS}} = 0.01$, and we emit a gluon g_1 from the qq dipole at a fixed shower evolution scale of $\ln v_1/Q = -20$, azimuthal angle $\phi_1 = 0$, and a few fixed values of $\bar{\eta}_{Q,1}$. We then examine the impact of a second gluon g_2, emitted at a scale $\ln v_2/Q = \ln v_1/Q - 2$, on the kinematics of g_1, varying $\bar{\eta}_{Q,2}$. Its azimuthal angle is fixed at $\phi_2 = 0$. We parameterise the available phase space of the emissions in terms of the Lund variables $\ln k_{t,i}/Q$ and η_i [78]. Some care has to be taken in defining these variables, in particular for emissions off the final-state quark. If only one gluon emission is present, we calculate two angular distances, one that parameterises the distance from the beam (d_{kB}), and one to the final-state quark (d_{kF})

$$d_{kB} = 1 - \cos\theta_k\,, \qquad d_{kF} = 1 - \cos\theta_{kq}\,. \tag{4.1}$$

where θ_k is the angle between k and the beam, while θ_{kq} is the angle between k and the final-state quark q, both defined in the Breit frame. We then define the angle

$$\cos\theta \equiv \begin{cases} +\cos\theta_{kq} & \text{if } d_{kF} < d_{kB}\,, \\ -\cos\theta_k & \text{if } d_{kF} > d_{kB}\,, \end{cases} \tag{4.2}$$

so that the Lund variables read

$$\eta = \frac{1}{2}\ln\frac{1+\cos\theta}{1-\cos\theta}\,, \qquad \ln\frac{k_t}{Q} = \frac{1}{2}\ln\frac{E_k^2(1-\cos^2\theta)}{Q^2}\,. \tag{4.3}$$

The sign in eq. (4.2) is chosen such that partons in the current hemisphere have positive rapidity, while partons in the remnant hemisphere have negative rapidity. Now let us move to the case where two gluons are present. In this case, we first calculate the angular distances of eq. (4.1) for both gluons. Focusing on emissions on the primary Lund plane, there are two possible scenarios: the smallest angular distance can either be to the beam, or the final-state quark. Note that the third scenario, where the second gluon is closest to the first emitted gluon, is instead described by a secondary Lund plane, which is not considered here. If the smallest angular distance is d_{k_iB}, we simply use the definition of the Lund variables of eq. (4.3) for both gluon emissions. If instead the smallest angular distance is between any of the two gluons and the final-state quark, we merge them into a new 'final-state' momentum p_F^μ. We then recalculate d_{kF} using that momentum, and calculate the new Lund variables for the last recombined emission.

Notice that this definition of the Lund variables shares some similarities with the variables associated with the generalisation of the Cambridge/Aachen algorithm for DIS, detailed in Appendix C. The main differences are first that for the current case, we are only interested in describing the 'primary' Lund plane, ignoring the case where the two emissions would first cluster together, as we want to focus on the case in which the emissions are widely separated in angle. Secondly, to define the transverse momentum of the splitting
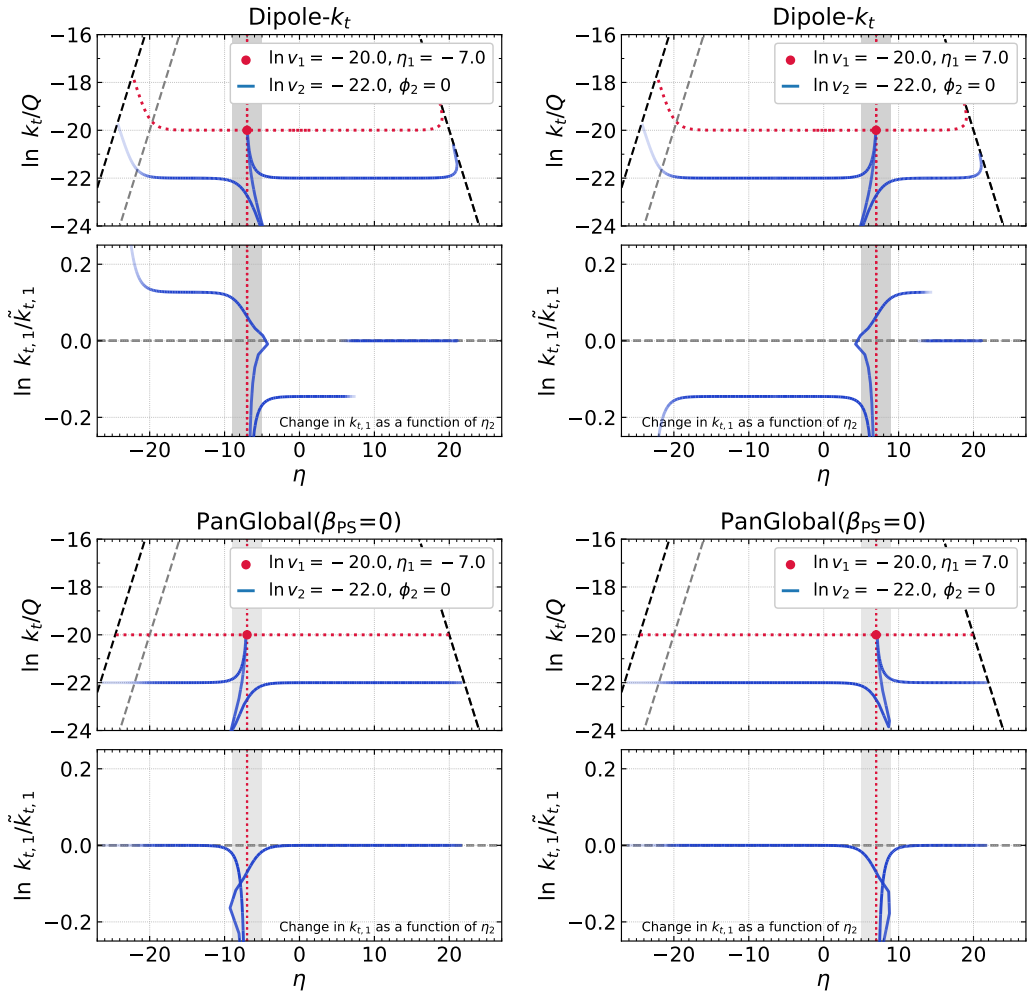
Figure 2: Double-emission contours for Dipole-k_t (top) and PanGlobal($\beta_{\text{PS}} = 0$) (bottom) for a first soft-collinear emission in the remnant hemisphere (left) and in the current hemisphere (right) for a DIS process with $x_{\text{DIS}} = 0.01$ and an incoming proton with negative rapidity in the Breit frame. The phase-space contours are shown as a function of $\ln k_t/Q$ and η. A red dot indicates the kinematics of the first emission which is fixed at $\eta_1 = -7$ (left) or $\eta_1 = 7$ (right) and $\ln v_1/Q = -20$ (in the plot labels, values of v_i are always expressed in units of Q). The contour of the first emission, obtained by fixing $\ln v_1/Q$ but varying η_1, is shown with the mostly horizontal red dotted line. That of the second emission at $\ln v_2/Q = -22$ is drawn as a blue solid line. The colour shading of the lines indicates the branching probability. In the bottom panels, we show the logarithm of the ratio between the transverse momentum of the first emission after ($k_{t,1}$) and before the second emission took place ($\tilde{k}_{t,1}$). This is expected to be zero (dashed grey line) except when the two emissions are close in rapidity (grey vertical band, where the rapidity of the first emission is indicated with a vertical red dotted line).

– 16 –
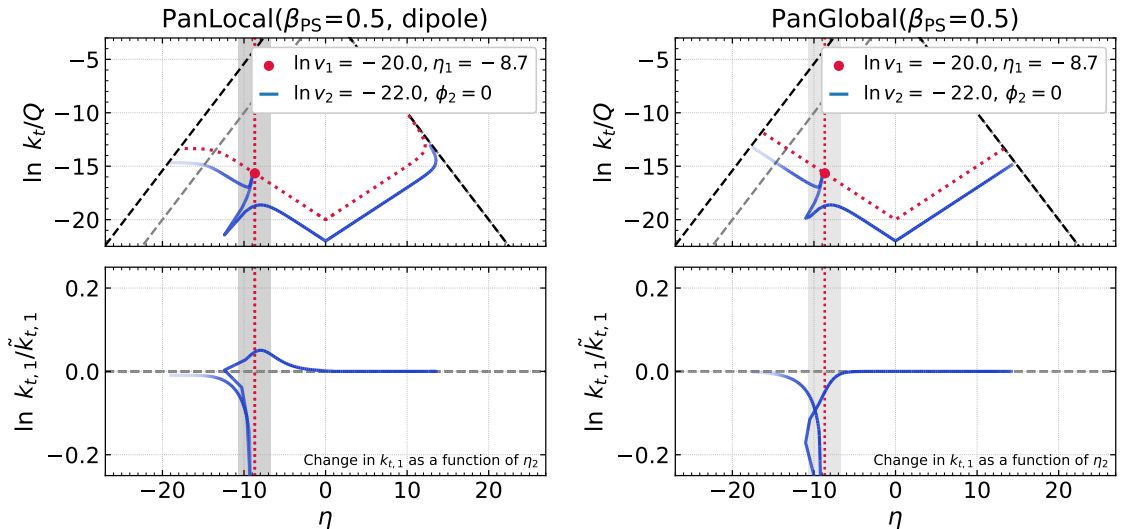
Figure 3: Same as Fig. 2, but for PanLocal($\beta_{\mathrm{PS}} = 0.5$, left) and PanGlobal($\beta_{\mathrm{PS}} = 0.5$, right) for $\eta_1 = -8.7$.

we always use the energy of the radiated gluon, while in the flavour-blind algorithm of Appendix C we take the energy of the softest parton.

On the top two panels of Fig. 2 we illustrate the two-emission contours for Dipole-k_t, a transverse-momentum ordered shower. We notice that the first emission erroneously takes the transverse-momentum recoil if

$$\eta_2 < \frac{1}{2}\left(\eta_1 - \ln \frac{v_1}{Q}\right). \tag{4.4}$$

This is because this shower uses a fully local map, such that the first gluon always absorbs the recoil whenever the second emission comes from the new initial-final ($q_I g_1$) dipole in the region $\eta_2 < \eta_1$, and because the midpoint of the final-final dipole is assigned in the dipole frame in the region where $\eta_2 > \eta_1$.

This behaviour can be corrected by either choosing a different evolution variable, or by conserving the transverse momentum globally, as done by the PanGlobal($\beta_{\mathrm{PS}} = 0$) shower. As discussed in Sec. 3.2.1, the global boost that takes care of redistributing the transverse momentum imbalance has the property of affecting mostly those partons at very large (and positive) rapidity, while leaving the ones living in the remnant hemisphere unchanged. Indeed, the bottom two panels of Fig. 2 show that subsequent emissions widely separated in rapidity leave the Lund variables associated with the first emission unaffected. The results obtained after taking a different ordering variable are shown in Fig. 3 for PanGlobal($\beta_{\mathrm{PS}} = 0.5$) and PanLocal. Here the ordering variable is set to $v \approx k_t e^{-\beta_{\mathrm{PS}}|\eta|}$, with $\beta_{\mathrm{PS}} = 0.5$. As already discussed in Ref. [38] local transverse-momentum conservation requires one to choose $\beta_{\mathrm{PS}} > 0$.

Finally in Fig. 4 we show results when choosing a different value for η_1 resulting in a hard-collinear first emission. They are analogous to the case where the first emission is
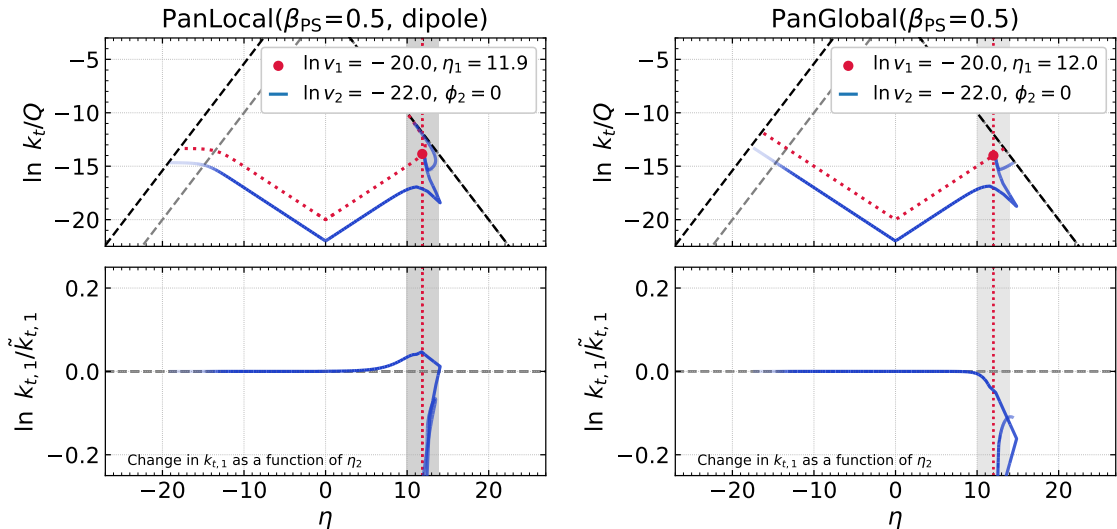
Figure 4: Same as Fig. 3, but considering a hard-collinear first emission with $\eta_1 = 12$.

soft-collinear, but note that care has to be taken for the PanLocal shower. At variance with the PanGlobal($\beta_{PS} = 0.5$) case, for very collinear initial-state radiation the ordering variable for PanLocal behaves like a transverse momentum. As discussed in Ref. [43] and in Sec. 3.2.2 around eq. (3.25), this modification in the local shower is necessary to prevent a very hard-collinear emission from significantly impacting the momentum of a softer previous emission.

We conclude that in the DIS PanScales showers, conversely to standard dipole showers, emissions widely separated in angle leave the kinematics of the previous emissions untouched. The novelty of our showers is that the transverse-momentum recoil due to initial-state-radiation is effectively absorbed by hard partons in the current hemisphere, while soft partons or partons collinear to the initial state remain unaffected, as required from colour coherence.

4.2 Subleading-colour corrections

Dipole showers are developed using the large-N_C approximation of QCD, and designed to correctly describe not only collinear emissions, but also soft wide-angle gluon emissions in the large-N_C limit. In standard dipole showers, subleading-colour corrections are included by replacing $C_A/2 = N_C/2$ with $C_F = (N_C^2 - 1)/(2N_C)$ when a quark leg is identified as emitter (we refer to this as the colour-factor-from-emitter scheme, CFFE). It has been known for quite some time [7] that this choice is inconsistent with colour coherence and more recently [39] it was observed that it leads to wrong (subleading-colour) contributions already at LL, due to the incorrect assignment of the emitter. Since $1/N_C^2 \sim \alpha_s$, these LL mistakes have the same size of NLL terms, so it stands to reason that these subleading colour terms should be included in an NLL-accurate shower.

Two schemes that do result in full-colour accuracy for LL terms were introduced in Ref. [79] for showers applicable to e^+e^- collisions, which also have been generalised for

colour-singlet production at hadron colliders in Ref. [43]: the so-called segment and NODS schemes. These schemes furthermore result in correct full-colour accuracy at NLL in the case of global observables, and next-to-double-logarithmic (NDL) accuracy for jet multiplicity, the latter of which is sensitive to the integrated rate of double-soft energy-ordered emissions at commensurate angles. The segment colour scheme divides each dipole into an arbitrary number of distinct segments, identified through the generation variable $\bar{\eta}_Q$. These segments either have a C_F or $C_A/2$ colour factor, and are assigned respecting colour coherence. The nested-ordered-double-soft (NODS) scheme was designed to not only get the correct integrated rate of two soft and energy-ordered emissions that occur at commensurate angles, but also describe them correctly at the differential level. This is achieved by applying a matrix element correction that describes a pair of energy-ordered commensurate-angle emissions, well separated in rapidity from all other emissions. For more details on these schemes, see Refs. [43, 79]. These algorithms are straightforwardly extended to the DIS case.

To validate these schemes for DIS, we perform tests of the differential matrix element produced by the shower after two strongly-ordered emissions. The kinematics of the first emission (which can either be a quark or a gluon) is fixed at $\eta_1 = -5$, $\phi_1 = 0$ and $\ln v_1/Q = -10$. The second emission is then emitted at a fixed value for $\ln v_2/Q = -60$, and sampled over $\bar{\eta}_{Q,2}$ and ϕ_2. The resulting shower predictions are then compared with the analytic result at full colour (FC).

In Fig. 5 we show the results obtained with PanGlobal($\beta_{\mathrm{PS}} = 0$) shower employing the segment, NODS and CFFE colour schemes. The emission density on the primary and secondary Lund plane are shown in terms of the rapidity η of the second emission, and its azimuthal angle ψ. These variables are defined according to our generalised DIS Cambridge-Aachen algorithm (Appendix C). Specifically, for emissions in the primary Lund plane, we define $\psi = \phi_2 - \phi_1 + \pi$ (or $\psi = \phi_2 - \phi_1 - \pi$, if $\phi_2 - \phi_1$ is larger than π). For emissions in the secondary Lund plane we instead use

$$\psi = \arctan \frac{\phi_2 - \phi_1}{\eta_2 - \eta_1} + \pi. \tag{4.5}$$

Let us first focus on the ratio between the parton shower and the analytic LC result, obtained using $C_A = 2C_F = 3$. These are illustrated in the upper set of panels (coloured green-blue). For the majority of phase space, the value of this ratio is either 1 or 8/9, when the effective colour factor is either $C_A/2$ or C_F. The lower set of panels (coloured red-white-blue) shows the ratio between the parton shower and the analytic FC result. As expected, the segment scheme assigns the correct colour factor everywhere except for the region where the second gluon is close in angle to the first emission. Note however that these deviations integrate to 0 after averaging over the angular phase space, therefore the all-order validations in Sec. 5 would not be sensitive to this effect. The NODS colour scheme corrects for this effect and produces the analytic differential matrix element also in the region where a pair of energy-ordered emissions occur at commensurate angles. The last set of plots shows the deviation from the CFFE scheme, which is currently implemented in standard dipole showers. This results in a wrong colour assignment over a region in phase
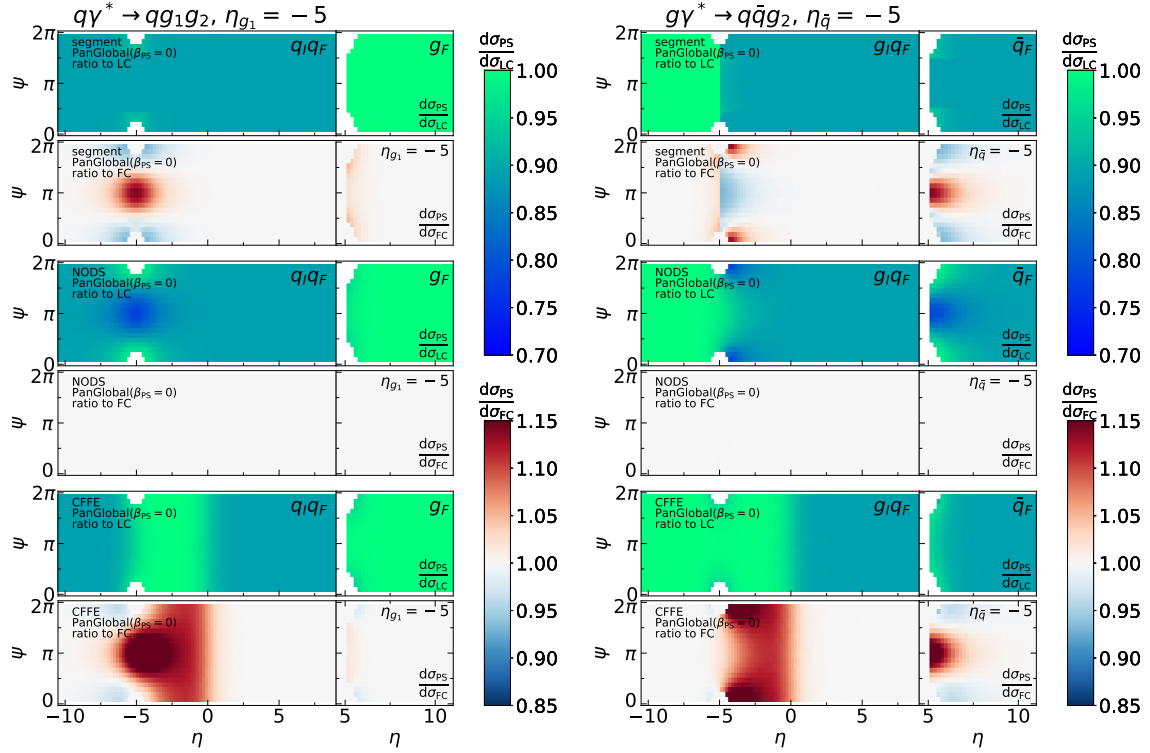
Figure 5: Density for the emission of an ultra-soft gluon from a $q\gamma^* \to qg_1$ configuration (left), or from a $g\gamma^* \to q\bar{q}$ system (right). In both cases, the incoming parton has a negative rapidity in the Breit frame, the final-state quark a positive one, and the first-emitted final-state parton (g_1 in the left pane, $\bar{q}$ in the right one) has a rapidity $\eta_1 = -5$. The emission density is illustrated as a function of the Lund variables η and ψ (defined in the main text). For each configuration, the left panel corresponds to the primary Lund plane, while the right panel represents the secondary Lund plane (populated by emissions from the parton located at $\eta_1 = -5$, see Appendix C). From top to bottom, the three rows show the results for the PanGlobal($\beta_{\mathrm{PS}} = 0$) shower result with the segment, NODS and CFFE colour scheme implemented For each row, the upper panel illustrates the ratio between the parton shower differential cross section and the leading colour (LC) result, $\mathrm{d}\sigma_{\mathrm{PS}}/\mathrm{d}\sigma_{\mathrm{LC}}$, obtained setting $C_A = 2C_F = 3$, while the lower panels show the deviation from the full colour (FC) differential matrix element, $\mathrm{d}\sigma_{\mathrm{PS}}/\mathrm{d}\sigma_{\mathrm{FC}}$.

space that is logarithmically extended. Hence this will result in a wrong LL term at FC, as already pointed out in Ref. [39].

Note that although here we have only shown results for the PanGlobal($\beta_{\mathrm{PS}} = 0$) shower, analogous results can be obtained for PanGlobal($\beta_{\mathrm{PS}} = 0.5$) and PanLocal. Similar considerations also apply to the Dipole-k_t shower. However, the fraction of phase space that has the wrong subleading colour corrections in the CFFE scheme is larger, as the emitter is chosen by partitioning the dipole frame, instead of in the Breit frame.

5 All-order validation

In this section, we investigate the all-order behaviour of the PanScales showers for DIS over a broad range of observables, targeting distinct classes of next-to-leading logarithmic effects, i.e. those of the form $\alpha_s^n L^n$. In Sec. 5.1 we test the capability of the showers to reproduce the DGLAP evolution of the parton distribution functions at single-logarithmic (SL) accuracy, which probes nested emissions in the hard-collinear region. In Sec. 5.2 we focus on the average particle multiplicity at next-to-double-logarithmic accuracy (NDL), targeting nested emissions in both the soft and collinear regions. In Sec. 5.3 we compare the shower cumulative cross section against the NLL predictions for several continuously-global observables, which is the only test sensitive to both double- and single-logarithmic terms in the Sudakov exponentiation (including running coupling effects), created through soft and collinear emissions. Finally, in Sec. 5.4 we study a non-global observable at SL accuracy, which probes the description of soft large-angle emissions in the shower. In Appendix E we comment on the size of NNLL corrections.

For each observable, we compare the shower's predictions to the known resummation. Subleading colour corrections are accounted for using the NODS scheme. Although it is possible to include spin correlations (see Appendix F), this is not done for the tests described below as none of the observables is sensitive to them at our targeted accuracy.
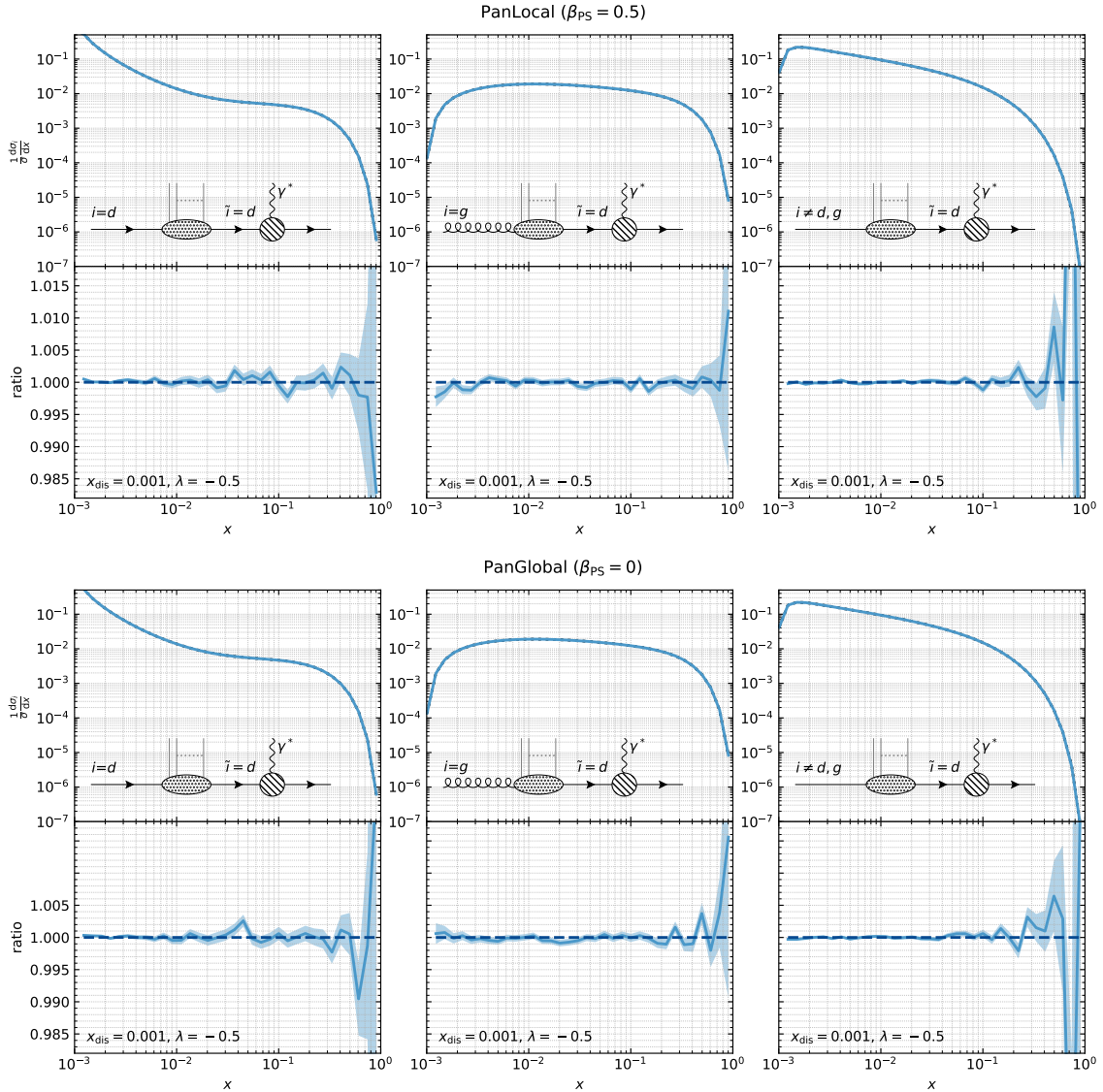
5.1 DGLAP evolution

Here we test the capability of our showers to reproduce the DGLAP [80–82] evolution of parton distribution functions (PDFs). More specifically, we fix the starting point of the shower to be the tree-level DIS process $q\gamma^* \to q$, where the incoming quark q is a down quark and has an energy fraction x_{DIS}, the photon has a space-like momentum equal to q_{DIS} with $Q^2 = -q_{\text{DIS}}^2$, and we run our showers from the scale Q until a given transverse-momentum cutoff $p_{t,\text{cut}} = Qe^L$. This cutoff is applied to the scale used as the argument of the running coupling, and it corresponds to the ordering-scale v for Dipole-k_t, and to $\kappa_\perp$ defined in eq. (3.9) for the PanScales showers. The flavour and energy fraction of the original quark extracted from the proton can change throughout the shower evolution. When the showering terminates the parton extracted from the proton will have a flavour denoted by i, and an energy fraction $x \geq x_{\text{DIS}}$. The dominant term of the distribution over i, x is SL $((\alpha_s L)^n$ with $L = \ln p_{t,\text{cut}}/Q$. The expected distribution will take the form

$$\frac{1}{\sigma}\frac{d\sigma_i}{dx} = \frac{1}{f_q(x_{\text{DIS}}, Q^2)} \int_{x_{\text{DIS}}}^1 \frac{dz}{z} D_{qi}(z, \alpha_s L) f_i\left(\frac{x_{\text{DIS}}}{x}, p_{t,\text{cut}}^2\right) \delta\left(\frac{x_{\text{DIS}}}{x} - z\right), \qquad (5.1)$$

where $f_j(y, \mu^2)$ is the density of partons of flavour j, carrying momentum fraction y at a factorisation scale μ. The (single-logarithmic) DGLAP evolution operator $D_{ij}(z, \alpha_s L)$ is defined such that the parton density functions satisfy

$$f_q(x, \mu^2) = \sum_j \int_x^1 \frac{dz}{z} z\, D_{qj}(z, \alpha_s L) f_j\left(\frac{x}{z}, p_{t,\text{cut}}^2\right). \qquad (5.2)$$

Figure 6: The ratio of the DGLAP evolution produced by the PanLocal($\beta_{\mathrm{PS}} = 0.5$) (upper panel) and PanGlobal($\beta_{\mathrm{PS}} = 0$) (lower panel) showers versus the DGLAP evolution as calculated with HOPPET. The results are shown as a function of the momentum fraction x carried by the parton i extracted from the proton. We fix the underlying Born DIS process to have a d quark in the initial-state with $x_{\mathrm{DIS}} = 0.001$, and fix $\alpha_s = 5 \cdot 10^{-6}$ with $\lambda = \alpha_s L = -0.5$. The three columns show different extracted flavours i that can lead to a d quark with energy fraction x_{DIS} entering the hard scattering process: we have a d quark on the left panel, a gluon in the middle panel, and any other flavour in the right panel.

In Fig. 6 we illustrate the results for the PanLocal($\beta_{\mathrm{PS}} = 0.5$) and PanGlobal($\beta_{\mathrm{PS}} = 0$) showers. The other showers, PanGlobal($\beta_{\mathrm{PS}} = 0.5$) and Dipole-$k_t$, lead to analogous results. The DGLAP reference prediction is obtained with HOPPET [83] at single logarithmic accuracy, probing only those initial conditions that lead in the evolution to $\delta_{\tilde{\imath}i}\delta(x - x_{\mathrm{DIS}})$

at the hard scale $\mu_{\text{F}} = Q$, with $x_{\text{DIS}} = 0.001$ and $\tilde{\imath}$ is a d quark. The shower runs are performed by fixing the underlying Born process to contain a d quark in the initial-state with $x_{\text{DIS}} = 0.001$, and the running of the strong coupling is performed at one loop. We show results obtained by setting $\alpha_s(Q) = 5 \cdot 10^{-6}$ and a large value of $L = -10^5$ ($\lambda = -0.5$), which sets any terms beyond SL accuracy to zero. To further speed up the calculation we discard radiation with a momentum fraction below some finite but small threshold e^{-11}, and only keep radiation with an absolute rapidity larger than 18 (i.e. very collinear to the initial- or final-state quark). We have verified that these cuts do not impact the results. Further details on the treatment of the PDFs may be found in Appendix A of Ref. [44]. We see that agreement with the HOPPET predictions is obtained for all showers to within the statistical accuracy (below 0.1% for the majority of the x range).

5.2 Particle multiplicity

In this section, we examine the shower's ability to reproduce the analytic prediction of the average particle multiplicity given the shower's transverse-momentum cutoff. Although particle multiplicity is not an infrared-safe quantity, the resummation structure of particle multiplicity, defined with an infrared cutoff, can be related to that of subject multiplicity at NDL, which is theoretically well-defined, and does not depend on the jet algorithm (as long as it is infrared safe). The logarithmic accuracy of particle multiplicity needs to be determined at the level of the distribution rather than the logarithm of the distribution. For such non-exponentiating observables, one writes

$$\langle N_{\text{NDL}}(\alpha_s, \xi) \rangle = h_1(\xi) + \sqrt{\alpha_s} h_2(\xi) \,, \tag{5.3}$$

with $\xi = \alpha_s L^2$ and where h_1 collects double-logarithmic (DL) $\mathcal{O}(\alpha_s^n L^{2n})$ terms, and $\sqrt{\alpha_s} h_2$ the next-to-double logarithmic (NDL) $\mathcal{O}(\alpha_s^n L^n)$ terms. At the desired level of accuracy (NDL), the average multiplicity obtained by counting the number of emissions generated by the shower with a transverse-momentum cutoff $p_{t,\text{cut}} = Q e^L$ (or equivalently, a shower that uses a strong coupling equal to zero below a given value of $p_{t,\text{cut}}$) is equivalent to that obtained after using a well-defined jet algorithm. The logarithm that is resummed then takes the form $L = \ln p_{t,\text{cut}}/Q$.

For the process at hand, if we fix the Born flavour to be $\tilde{\imath} = q$, we have [84–86]
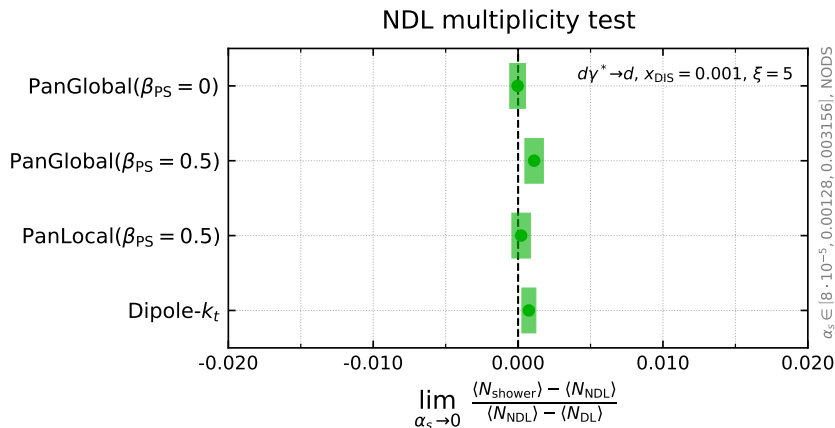
$$h_1(\xi) = \frac{2C_F}{C_A} \left[\cosh \nu - 1 \right] + N_b \,, \tag{5.4a}$$

$$h_2(\xi) = \sqrt{\frac{1}{2\pi C_A}} \sinh \nu \, \frac{Q^2 \partial \ln f_q(x_{\text{DIS}}, Q^2)}{\partial Q^2} + \frac{2C_F}{C_A} \left[\frac{\beta_0}{2} \sqrt{\frac{\pi}{2C_A}} \left(\nu \cosh \nu + (\nu^2 - 1) \sinh \nu \right) \right.$$
$$+ \sqrt{\frac{C_A}{2\pi}} B_{gq} \left(\frac{2C_F - C_A}{C_A} \nu \cosh \nu + \frac{5C_A - 6C_F}{C_A} \sinh \nu + 4 \frac{C_F - C_A}{C_A} \nu \right)$$
$$\left. + \sqrt{\frac{C_A}{2\pi}} \left(2 B_{qq} \sinh \nu + B_{gg} \left(\nu \cosh \nu - \sinh \nu \right) \right) \right] \,, \tag{5.4b}$$

with $N_b = 1$ the number of final-state partons at LO, and

$$\nu = \sqrt{\frac{2C_A \xi}{\pi}} \,, \quad B_{gg} = -\frac{11}{12} \,, \quad B_{qq} = -\frac{3}{4} \,, \quad B_{gq} = \frac{2n_F}{3C_A} \,, \quad \beta_0 = \frac{11C_A - 2n_F}{12\pi} \,. \tag{5.5}$$

Figure 7: Extrapolation of $\frac{\langle N_{\mathrm{shower}}(\alpha_s,\xi)\rangle - \langle N_{\mathrm{NDL}}(\alpha_s,\xi)\rangle}{\langle N_{\mathrm{NDL}}(\alpha_s,\xi)\rangle - \langle N_{\mathrm{DL}}(\alpha_s,\xi)\rangle}$ for $\alpha_s \to 0$ at fixed value of $\xi = \alpha_s L^2 = 5$ for several showers considering the DIS process $d\gamma^* \to d$ with $x_{\mathrm{DIS}} = 0.001$.

As before, f_q denotes the PDF of the incoming parton at LO, which carries an energy fraction x_{DIS}.

At DL accuracy, this test probes the soft-collinear nested structure of the shower. To reproduce the average multiplicity at NDL, the parton shower must also correctly incorporate hard-collinear corrections to the splitting functions (corresponding to the second and third line of Eq. (5.4b)), the running of the coupling constant (first line of Eq. (5.4b)), the DGLAP evolution of the PDF (last line of Eq. (5.4b)), and the colour terms. The treatment of these contributions is the same across all showers, hence we expect to see agreement. The parton shower correctly reproduces the analytic expectation at NDL if the ratio

$$\frac{\langle N_{\mathrm{shower}}(\alpha_s,\xi)\rangle - \langle N_{\mathrm{NDL}}(\alpha_s,\xi)\rangle}{\langle N_{\mathrm{NDL}}(\alpha_s,\xi)\rangle - \langle N_{\mathrm{DL}}(\alpha_s,\xi)\rangle} \,, \tag{5.6}$$

vanishes in the $\alpha_s \to 0$ limit, where ξ is kept fixed and $\langle N_{\mathrm{DL}}(\alpha_s,\xi)\rangle$ corresponds to Eq. (5.3) with h_2 set to 0. To extract the $\alpha_s \to 0$ limit, we run the PanScales showers for the DIS process $q\gamma^* \to q$, where we set $q = d$, $x_{\mathrm{DIS}} = 0.001$, $\xi = 5$ and sample $\alpha_s = \left\{8 \cdot 10^{-5}, 0.00128, 0.003156\right\}$, performing a quadratic polynomial extrapolation to get the $\alpha_s \to 0$ result. Systematic uncertainties are estimated performing an alternative extrapolation with $\alpha_s = 0.00512$ instead of $\alpha_s = 0.003156$, and added in quadrature to the statistical uncertainty. Like in the previous section, the running of the coupling constant is performed at one loop, as the 2-loop running only enters at NNDL accuracy. Subleading colour corrections are included using the NODS scheme. The obtained result is shown in Fig. 7. We notice that all the showers are consistent with the NDL expectation, with an uncertainty well below 0.1%.

5.3 Continuously-global observables

This section details tests on a range of global [87] observables. The cumulative distribution of such observables, i.e. the probability that the observable O takes a value smaller than

e^L, can be written as a function of $\lambda = \alpha_s L$, and takes the form

$$\Sigma(O < e^L) = H(\alpha_s) \exp\left[-L\, g_1(\lambda) + g_2(\lambda) + \dots\right] + \dots ,\tag{5.7}$$

where g_1 contains the LL, and g_2 the NLL contribution. The function $H(\alpha_s)$ is the hard function, which can be set equal to 1 at our targeted NLL accuracy. To test the accuracy of the shower we examine

$$\lim_{\alpha_s \to 0} \frac{\Sigma_{\mathrm{PS}}(\lambda) - \Sigma_{\mathrm{NLL}}(\lambda)}{\Sigma_{\mathrm{NLL}}(\lambda)} ,\tag{5.8}$$

at a fixed value of λ, which should tend to 0 if the shower is NLL accurate. To extract the $\alpha_s \to 0$ limit, we need to run the shower at very small α_s values. We are able to do so thanks to the numerical techniques developed in Refs. [38, 44, 79]. These techniques assume that in the soft-collinear limit, the observable scales as

$$O \sim \frac{p_T}{Q} e^{-\beta_{\mathrm{obs}}|\eta|} ,\tag{5.9}$$

where $\beta_{\mathrm{obs}} \geq 0$ is a constant number. This implies that we can only consider continuously-global observables [87] in our tests.

Keeping this technical limitation in mind, to test our showers, we introduce three sets of observables, parameterised by $\beta_{\mathrm{obs}} \in [0, 0.5, 1]$:

$$S_{p,\beta_{\mathrm{obs}}} = \sum_{j \in \mathrm{partons}} \frac{k_{t,j} e^{-\beta_{\mathrm{obs}}|y_j|}}{Q} ,\tag{5.10a}$$

$$S_{j,\beta_{\mathrm{obs}}} = \sum_{j \in \mathrm{jets}} \frac{k_{t,j} e^{-\beta_{\mathrm{obs}}|y_j|}}{Q} ,\tag{5.10b}$$

$$M_{j,\beta_{\mathrm{obs}}} = \max_{j \in \mathrm{jets}} \frac{k_{t,j} e^{-\beta_{\mathrm{obs}}|y_j|}}{Q} .\tag{5.10c}$$

For the particle observable $S_{p,\beta_{\mathrm{obs}}}$, the sum over j runs over all partons, and $k_{t,j}$, y_j correspond to the transverse momentum and the rapidity of the parton in the Breit frame. Jets are defined with the algorithm detailed in Appendix C. For the two jet observables, the sum over j runs over all jets found inside the collection of beam jets and the final-state macro-jet. The $k_{t,j}$ and y_j are their primary Lund-plane coordinates. The analytic expectations for the observables quoted in Eq. (5.10) are collected in Appendix D. Note that $S_{p,\beta_{\mathrm{obs}}}$ will only be computed for $\beta_{\mathrm{obs}} > 0$, i.e. when its NLL prediction corresponds to the one of a standard additive observable and is equivalent to $S_{j,\beta_{\mathrm{obs}}}$. For $\beta_{\mathrm{obs}} > 0$ the contribution of the original hard final-state leg to $S_{p,\beta_{\mathrm{obs}}}$ is subleading and can be neglected, thus yielding the same result as $S_{j,\beta_{\mathrm{obs}}}$. This is no longer the case for $\beta_{\mathrm{obs}} = 0$, as recoil effects contribute at NLL. We stress that these observables are not directly measurable, because they are built from emissions in both the remnant and the current hemisphere, but they have the property of having a remarkably simple resummation structure at NLL. For this reason, they can be easily used to test the logarithmic accuracy of showers, but they can also be employed as resolution variables to build slicing methods [88, 89] or NNLO+PS matching prescriptions [19, 20, 22].
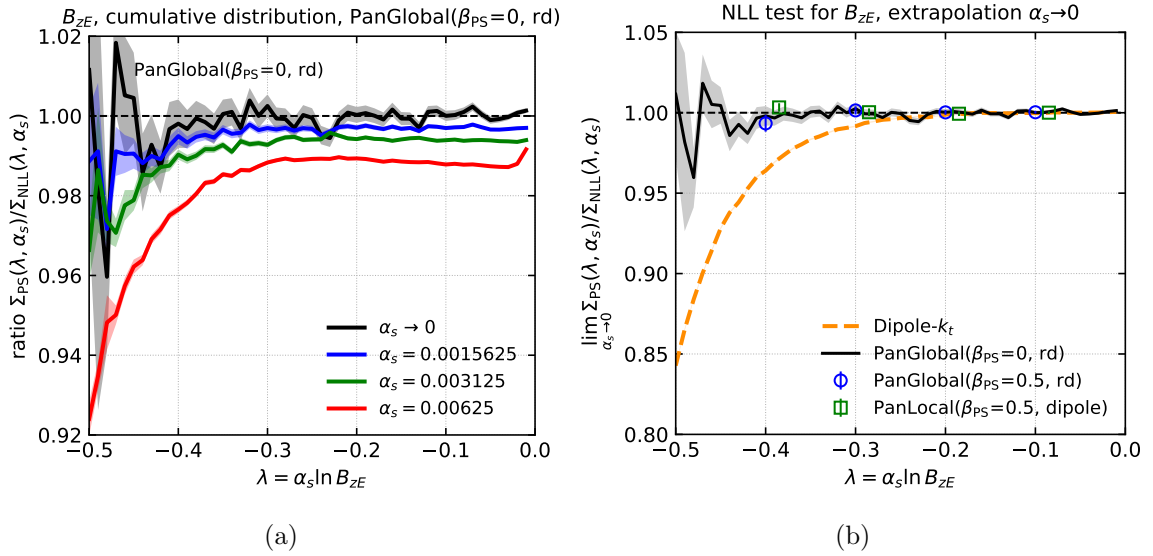
Figure 8: Cumulative distribution for the broadening normalised with respect to the energy in the current hemisphere, B_{zE}, for the process $q\gamma^* \to q$ with $x_{\text{DIS}} = 0.2$. In the left panel we show PanGlobal($\beta_{\text{PS}} = 0$) results, obtained with finite values of α_s, as well as the $\alpha_s \to 0$ extraction. In the right panel, we illustrate the $\alpha_s \to 0$ extraction for all the showers: the ratio with the analytic prediction must be 1 if the shower is NLL. Note that the values for the PanLocal shower have been shifted to the left to improve readability, i.e. their probed λ values coincide with those for PanGlobal($\beta_{\text{PS}} = 0.5$).

We further test our showers with observables that are phenomenologically accessible. To remove contamination from the fragmenting beams in the remnant hemisphere, allowing for a better experimental measurement, event shapes in DIS are often defined in the current hemisphere $\mathcal{H}_c$. Examples of such observables, which are continuously-global and satisfy the recursive infrared-safety requirement of Ref. [87], are

$$B_{zE} = \frac{\sum_{i \in \mathcal{H}_c} |\vec{p}_{\perp,i}|}{2 \sum_{i \in \mathcal{H}_c} |\vec{p}_i|} , \tag{5.11a}$$

$$B_{zQ} = \frac{\sum_{i \in \mathcal{H}_c} |\vec{p}_{\perp,i}|}{Q} , \tag{5.11b}$$

$$\tau_{zQ} = 1 - \frac{2 \sum_{i \in \mathcal{H}_c} |p_{z,i}|}{Q}, \tag{5.11c}$$

where all the quantities are defined in the Breit frame, and the suffix z implies they are measured with respect to the photon axis. The analytic predictions for the two definitions of broadening, B_{zE} and B_{zQ}, can be found in Ref. [90]. They are examples of $\beta_{\text{obs}} = 0$ observables, and their NLL prediction is identical. For τ_{zQ}, which is a $\beta_{\text{obs}} = 1$ observable, these predictions were computed in Ref. [73]. These results are also summarised in Appendix D.

In Fig. 8a we show the ratio of the PanGlobal($\beta_{\text{PS}} = 0$) prediction to the NLL result for the cumulative distribution of the broadening normalised with respect to the energy in
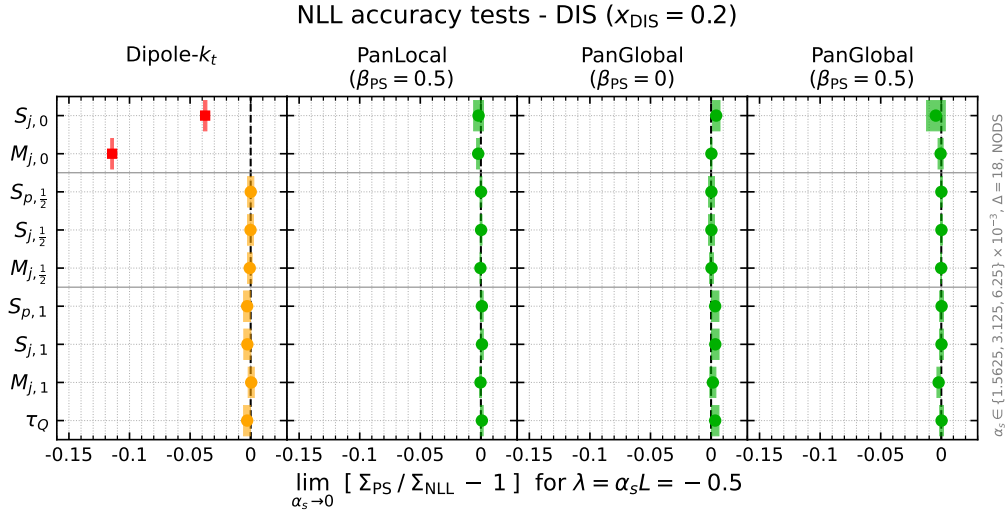
Figure 9: The $\alpha_s \to 0$ extrapolation of the deviation of the shower result from the NLL expectation for the process $q\gamma^* \to q$ with $x_{\mathrm{DIS}} = 0.2$ and $\lambda = -0.5$ for several continuously-global observables. The red colour signals a deviation from the analytic expectation larger than two standard deviations, while the green colour signals an agreement. When numerical agreement between the shower and the analytic resummation is found, but fixed-order issues are known, we use the amber colour.

the current hemisphere, B_{zE}, for increasingly smaller values of α_s,

$$\alpha_s = \{0.0015625, 0.003125, 0.00625\} \tag{5.12}$$

and $\lambda \geq -0.5$. The coloured band represents only the statistical uncertainty. More information on how these results are obtained is given in Appendix E. In black we illustrate the result of the $\alpha_s \to 0$ extrapolation, which has been performed with a quadratic interpolation. In Fig. 8b we summarise the $\alpha_s \to 0$ extractions for all the showers. From this figure it is clear that all the new PanScales showers for DIS processes reproduce the analytic expectation, while we observe deviations for Dipole-k_t reaching up to 15% for $\lambda = -0.5$. We obtain identical results for B_{zQ}, not shown here.

The shower's expectation for the other observables are summarised in Fig. 9, where we show the ratio with the NLL result for the cumulative distribution $\Sigma(O < e^L)$ in the $\alpha_s \to 0$ limit with $\lambda = -0.5$. Here, the central value is again obtained using the α_s values in eq. (5.12), but the uncertainty is given by summing in quadrature the statistical uncertainty and the difference between the central value and the one obtained by performing the extrapolation on the set of α_s values where $\alpha_s = 0.003125$ is replaced with $\alpha_s = 0.0125$.

The PanScales showers agree with the analytic expectations for all the observables. Dipole-k_t leads to manifestly wrong all-order results at NLL for $\beta_{\mathrm{obs}} = 0$ observables, with a 4% deviation for $S_{j,0}$ and a 12% deviation for $M_{j,0}$. Like in Refs. [38, 44], we observe that despite the fixed-order issue that we highlighted in Sec. 4.1, Dipole-k_t seems to reproduce the correct analytic expectations for $\beta_{\mathrm{obs}} > 0$. The NLL-violating terms manifest

themselves as super-leading logarithms that violate the exponentiation, as observed in Ref. [38], which however resum to 0 in the all-orders limit for $\beta_{\mathrm{obs}} > 0$.

5.4 Non-global logarithms

Many observables are sensitive to radiation in a restricted portion of the Lund plane. In the context of DIS, these observables are, for example, the current jet mass, the C-parameter, the thrust with respect to the current-hemisphere thrust-axis [91] and Q_t, i.e. the transverse momentum of the system comprising the partons in the current hemisphere [92]. For what concerns Higgs production in VBF, isolation criteria can be used to reduce this production mode from gluon fusion [62]. The resummation for these observables naturally involves non-global logarithms (NGLs) [93, 94], which can be correctly reproduced at leading-colour single-logarithmic (SL) accuracy only by dipole showers [6].

To assess the ability of our showers to reproduce such NGLs, we consider the scalar sum of the transverse momenta of the partons in a rapidity slice

$$S_\Delta^{\mathrm{slice}} = \frac{\sum_i k_{t,i}\Theta(|\eta_i| < \Delta)}{Q} \equiv \frac{k_{t,\mathrm{slice}}}{Q}\,, \tag{5.13}$$

where the transverse momentum $k_{t,i}$ and the rapidity η_i of the partons are defined in the Breit frame. NGLs for this observable are single-logarithmic terms of the form $\lambda^n = \alpha_s^n L^n$, created by soft large-angle emissions near the edge of the slice, i.e. near $y = \pm\Delta$.

Fig. 10a shows the comparison between the PanScales shower predictions with the expected results for $-0.5 \le \lambda < 0$ and $|y| < 1$, while in Fig. 10b we show the results for $\lambda = -0.5$. We generate our reference calculation in the large-N_{C} limit (with $C_F = C_A/2 = 3/2$) from the code developed for Ref. [95], which uses the strategy of Ref. [93]. The shower predictions are obtained running with $\alpha_s = 10^{-9}$, so that NSLs are numerically negligible. To reduce the parton multiplicity, without affecting the observable under consideration, we impose a rapidity and a soft-emission cut, vetoing radiation with $|\eta| > 13$ and $\ln k_t < \ln k_{t,\mathrm{slice}} - 18$. Furthermore, like in Secs. 5.1 and 5.2, the running of the coupling constant is performed at one loop, with $K = 0$, as these effects only enter at NSL/NNDL.

In all cases, we notice an excellent agreement between the PanScales showers and the correct SL distribution. This is true also for Dipole-k_t, despite fixed-order issues, exactly like in the case of continuously-global event shapes with $\beta_{\mathrm{obs}} > 0$.

6 Phenomenological results Higgs production in VBF

We now move to the PanScales showers for VBF, presenting some exploratory phenomenological results, and explaining more details on the implementation of such process in our framework. This channel provides a clean experimental signature and is therefore an ideal environment to study the Higgs boson.[10] As already explained in Sec. 3.3, at NLO the VBF channel can be seen as two independent DIS processes for each hadronic sector. The two jets that are formed after the initial-state quark emits a vector boson are typically produced with a large absolute rapidity. Colour coherence then results in little jet activity

---

[10]The VBF channel is also used to search for di-Higgs production at the LHC [96].
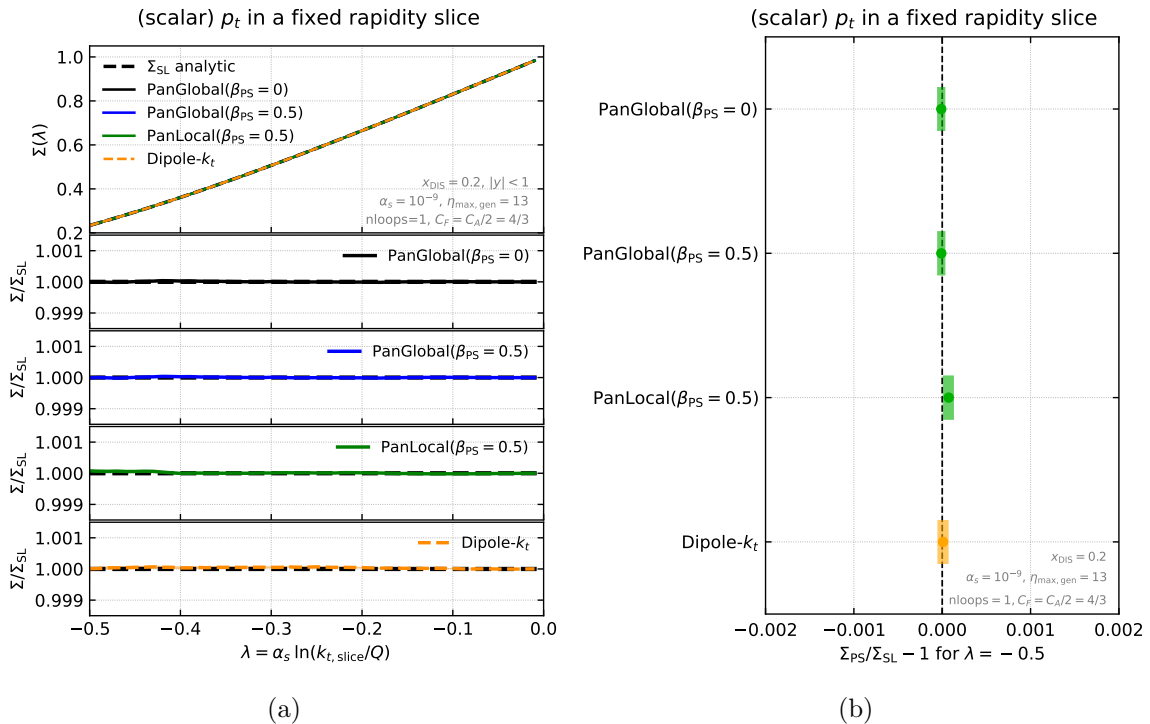
Figure 10: (a) Cumulative distribution for the transverse momentum in a rapidity slice of $|y| < 1$ as a function of $\lambda = \alpha_s \ln \frac{k_{t,\text{slice}}}{Q}$ for the PanScales showers and Dipole-k_t. The top panel shows the expected (black dashed) and the showers (solid) results, while the bottom panels show the ratio between the shower and the analytic prediction for each of the showers. (b) Relative difference between the shower Σ_{PS} and the expected single-logarithmic result (Σ_{SL}) for a fixed value of $\lambda = -0.5$ for all the PanScales showers. Colour coding is like in Fig. 9.

in the central rapidity region; radiation will be primarily concentrated around the two hard jets at (opposite) large rapidities.

For the phenomenological studies we produce the Higgs boson via the ZZ channel in a VBF topology with a centre-of-mass energy of 13.6 TeV. We run all showers using the NODS colour scheme, even though the CFFE scheme is the one adopted by standard dipole showers, to more faithfully gauge the kinematic differences between the LL and NLL showers. The hard process is obtained from PYTHIA8.3 [37] at LO accuracy, using the default values for the electroweak parameters and the Higgs mass. We use the NNPDF 4.0 LO PDF set with perturbative charm content [97] (LHAPDF label 332500 [98]), corresponding to $\alpha_s(m_Z) = 0.118$. The default factorisation and renormalisation scale used in PYTHIA8.3 to generate the hard process is

$$\mu_{F,h} = \mu_{R,h} \equiv \mu_h = \sqrt[3]{m_{T,H} m_{T,V_1} m_{T,V_2}}, \quad m_{T,i} = \sqrt{p_{\perp,i}^2 + m_i^2}, \tag{6.1}$$

where $V_{1,2}$ denote the vector-bosons exchanged in the t-channel propagators for each of the two hadronic sectors, and m_{H,V_1,V_2} the Higgs/vector-boson masses. However, as discussed

in Sec. 3.3, another choice would be to use the virtualities of the exchanged boson as two independent scales for the two hadronic sectors. To this end, we apply the reweighting factor

$$w = \frac{f_{i_1}(x_1, \mu_1) \ f_{i_2}(x_2, \mu_2)}{f_{i_1}(x_1, \mu_h) \ f_{i_2}(x_2, \mu_h)}, \tag{6.2}$$

where $f_{i_{1,2}}$ is the PDF of the incoming quark $i_{1,2}$, which carries an energy fraction $x_{1,2}$, and $\mu_{1,2} = \sqrt{Q_{1,2}^2}$. We start the parton shower at a distinct scale for each of the hadronic sectors, i.e.

$$v_{\max,i}^2 = Q_i^2 \frac{1 - x_i}{x_i} \ . \tag{6.3}$$

In practice, we use the maximum of the two values as common starting scale, and we perform a veto to ensure that $v < v_{\max,i}$ in each hadronic section.

We estimate the uncertainty stemming from renormalisation scale variations using a modified scheme for α_s [44, 99], that is

$$\alpha_s\left(\mu_R^2\right)\left(1 + \frac{\alpha_s\left(\mu_R^2\right)}{2\pi}K + 2\alpha_s\left(\mu_R^2\right)b_0(1-z)\ln x_R\right), \quad \mu_R = x_R \mu_{R,0}, \tag{6.4}$$

with $\mu_{R,0} = \rho v e^{\beta_{\mathrm{PS}} |\bar{\eta}_{Q_i}|}$ the central scale. The factor z is the fraction of the emitter-momentum carried away by the radiation. With this, $1 - z$ ensures that scale compensation at NLL is present for soft emissions, but not for hard emissions. We should omit this term for the LL-accurate shower Dipole-k_t, but we do include the CMW factor K by default. Renormalisation-scale variations are probed taking $x_R \in \{0.5, 1, 2\}$, and the infrared cutoff of the shower is implemented such that $\alpha_s(\mu_R^2) = 0$ for $\mu_R < x_R \times 0.5$ GeV. Factorisation-scale uncertainties are probed independently from the renormalisation scale, and are assessed using

$$\ln \mu_F \equiv \ln\left(x_F \mu_{F,0}\right) = \ln Q_i + \frac{1}{1 + \beta_{\mathrm{PS}}} \ln \frac{v_i}{Q_i} + \ln x_F, \tag{6.5}$$

with $x_F \in \{0.5, 1, 2\}$. In our results we show the 7-point scale variation, obtained by taking $(x_R, x_F) \in \{(1,1), (0.5,1), (1,0.5), (0.5,0.5), (2,1), (1,2), (2,2)\}$. It is important to note that stress that such variations typically do not capture all sources of uncertainty. Indeed, the showers feature different recoil schemes and evolution variables, which lead to subleading (uncontrolled) corrections, whose uncertainty is not captured in the above approach.

We use the anti-k_T algorithm [100] with $R = 0.4$, implemented in FASTJET [101] to cluster jets with the definition $p_{T,j} > 25$ GeV, $|\eta_j| < 4.5$, and consider two setups:

- "minimal cuts", where we require the presence of two resolved jets;

- "VBF cuts", where we require that the two leading jets (i.e. those two with the largest transverse momenta) are separated by a rapidity $\Delta\eta_{j_1 j_2} > 4.5$, have a dijet invariant mass of at least $m_{j_1 j_2} > 600$ GeV and lie in opposite hemispheres ($\eta_{j_1} \cdot \eta_{j_2} < 0$).
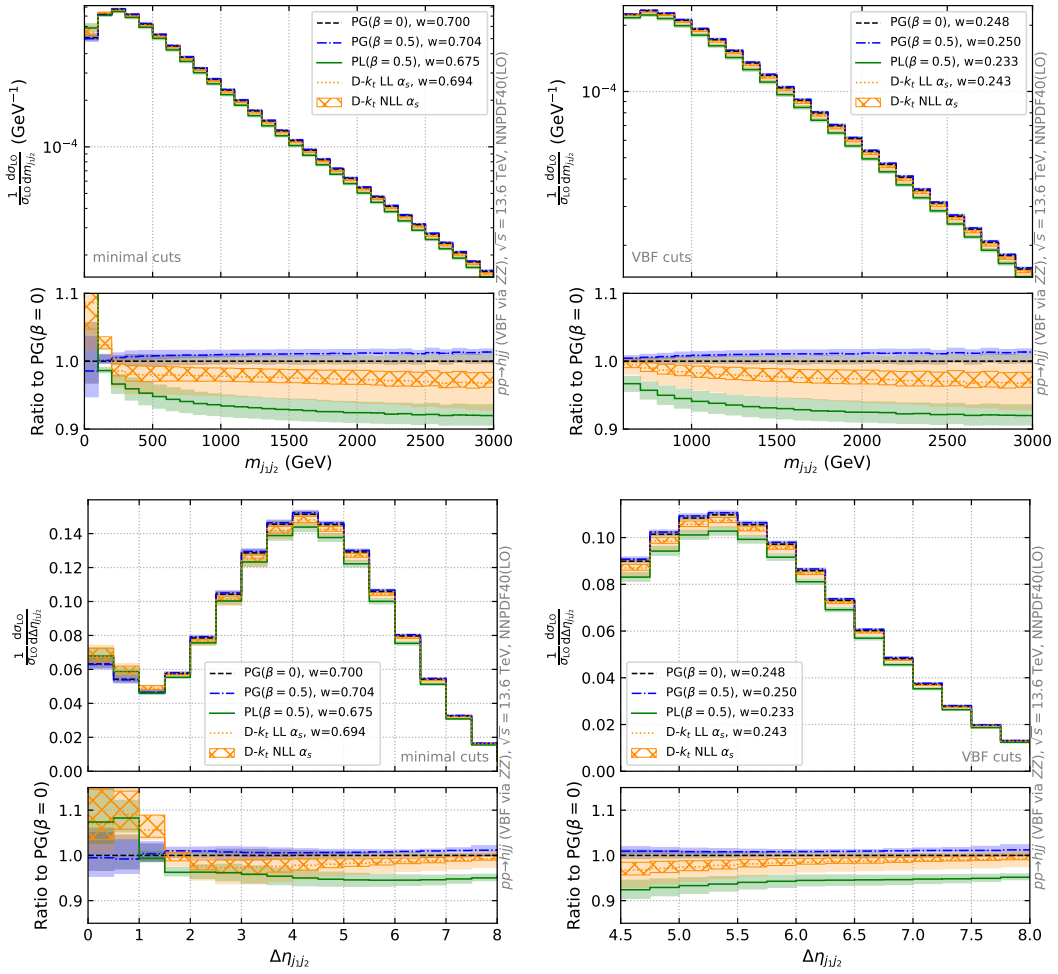
Figure 11: Distributions normalised to the total (before cuts) LO cross section σ_{LO} for $m_{j_1 j_2}$ (top) and $\Delta\eta_{j_1 j_2}$ (bottom) after applying the minimal selection cuts (left) and the VBF cuts (right). We show PanGlobal($\beta_{\mathrm{PS}} = 0$), black dashed, PanGlobal($\beta_{\mathrm{PS}} = 0.5$), blue dash-dotted, PanLocal($\beta_{\mathrm{PS}} = 0.5$), green solid and Dipole-k_t, orange, dotted. The label w indicates the total area under the curve. The vertical lines on the central value of each bin indicate the statistical uncertainty, which is mostly negligible and therefore not visible. The band indicates the renormalisation/factorisation scale uncertainty, obtained as explained after eq. (6.5). For Dipole-k_t the hashed band indicates the uncertainty obtained using the strong coupling for the shower as in eq. (6.5), whereas the solid band indicates the uncertainty obtained without the NLL scale-compensating term of eq. (6.5). The bottom panel shows the ratio with respect to the PanGlobal($\beta_{\mathrm{PS}} = 0$) result.

The results shown below do not include the simulation of beam remnants, hadronisation or multi-parton interaction. We have the option to incorporate them into our framework trivially using PYTHIA8.3, but we have made the decision not to do so. This choice enables us to provide a clearer comparison between the NLL PanScales showers and the LL-accurate Dipole-k_t shower. Note that comparisons with other publicly-available LL showers are not

being performed here, but we should stress that since we consider also regions where the prediction is not necessary dominated by logarithmic enhancements, differences between publicly-available showers and Dipole-k_t can be sizeable.

We first consider inclusive observables, i.e. those observables that are non-vanishing at LO. The value of these observables is primarily set by the hard scattering process, and the shower should impact these observables only marginally. In Fig. 11 we show two such observables: the invariant mass of the two leading jets $m_{j_1 j_2}$ and the rapidity seperation between them $\Delta\eta_{j_1 j_2}$. Uncertainties from renormalisation/factorisation scale variations are noticably smaller in the NLL showers than in Dipole-k_t. This is a direct consequence of including the scale-compensating term of eq. (6.4). In general, the scale uncertainties are small, except in the regions where $\Delta\eta_{j_1 j_2}$ and $m_{j_1 j_2}$ are small (see Fig. 11, left). These regions are contaminated by events where one of the two tagged jets actually originates from the shower hardest emission. Indeed, because of this effect, the scale uncertainties here are larger than in the bulk of the distribution. With the exception of these regions, which are excluded after applying the VBF cuts, it can be observed that differences between the NLL showers are of the order of $\mathcal{O}(5-10\%)$, i.e. commensurate with known NLO corrections. However, the spread of the NLL showers is much larger than their scale variation, and the latter indeed can then not be used to accurately and reliably capture the differences between the showers. The effect of adding the scale-compensating term in eq. (6.5) is sizeable: uncertainty stemming from scale variations increases by roughly a factor of two when turning off those scale-compensating terms. We do want to stress that turning off those terms underestimates the scale uncertainty for the Dipole-k_t shower. As this is not an NLL shower, and the scale-compensating term originates from an NLL prediction, we are not strictly allowed to turn off the compensating effect. We also notice that the LL shower lies in between the prediction of the PanScales NLL showers.

We now turn to observables that can only be defined in the presence of a third jet, and therefore are a clean probe of the shower's behaviour. In particular, we consider the pseudo-rapidity of the third jet, η_{j_3}, and the transverse momentum of the third jet p_{T,j_3}, as shown in Fig. 12. Colour coherence predicts a suppression of radiation in the central rapidity region. All the showers considered here indeed show this behaviour, as can be observed in the top panel of Fig. 12. In contrast to the previously-considered inclusive observables, we now see that the difference between using an LL effective running coupling in the shower or an NLL one is minimal. Indeed, the scale uncertainty bands are of roughly equal size for the two Dipole-k_t results. This is related to the fact that these observables are all dominated by the shower's hardest emission. For this emission, the uncertainty stemming from μ_F variations exceed that of that for μ_R variations. In addition, we note that Dipole-k_t typically lies above the predictions of the NLL showers. This can be mostly traced back to a diference in normalisation, as seen by comparing the weights w of the histograms of the NLL showers versus that of Dipole-k_t. These normalisation differences are due to the fact that Dipole-k_t tends to show a higher rate of 3-jet events than the other showers. This rate is controlled by the hard-emission phase-space region. However, since we do not include matching, this region is not controlled in our showers, and we leave a further detailed investigation of the differences between the LL and NLL showers for future
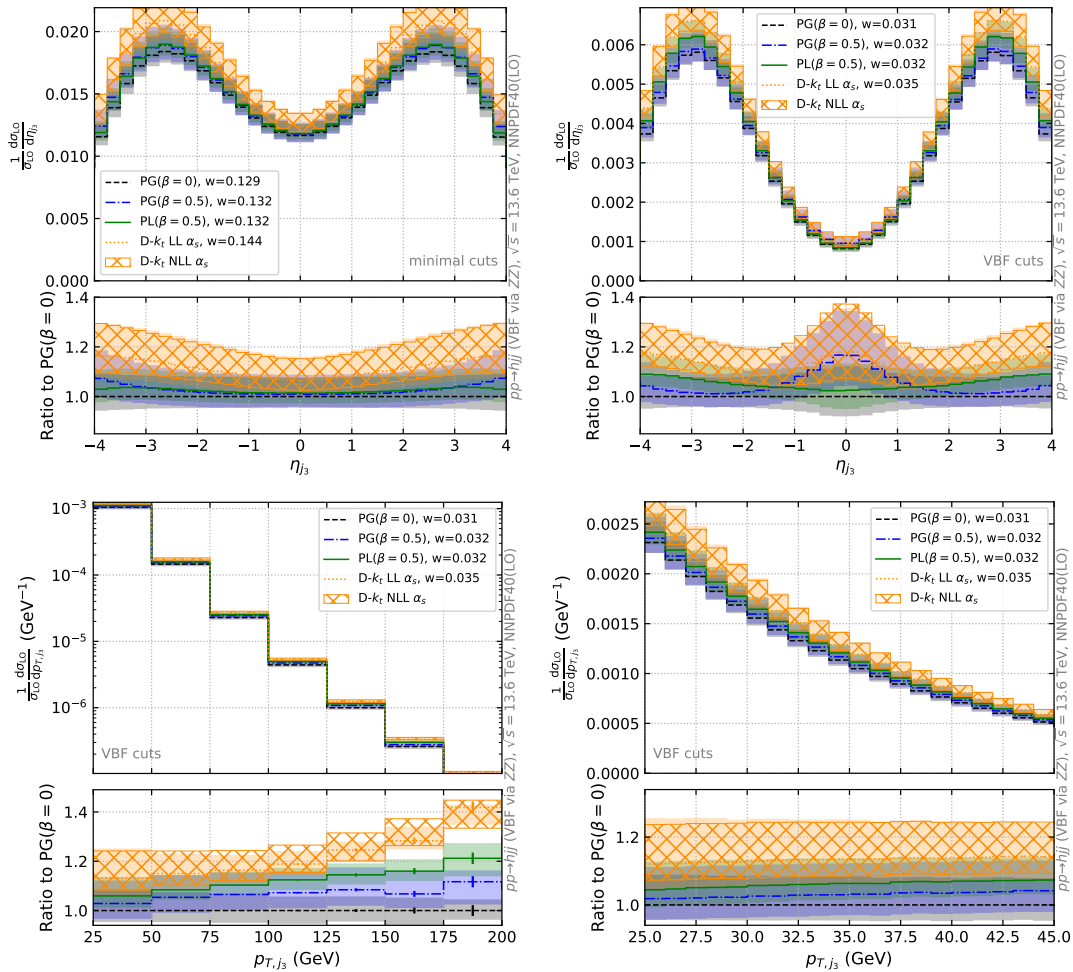
Figure 12: As Fig. 11 but for η_{j_3} (top), and p_{T,j_3} (bottom). For the latter we only show the result after applying the VBF cuts, and the right bottom panel shows a magnification of the (relatively) small transverse-momentum region.

work.

At this stage, we also refrain from performing a comparison with experimental data, for similar reasons: (I) NLO matching is not yet implemented; (II) we have not yet studied the interplay between our showers and non-perturbative effects; (III) we have not yet tuned our showers. We thus leave a theory-data comparison for future work.

7 Conclusions

In this work, we have introduced new NLL-accurate dipole showers for processes involving the exchange of a colour-singlet in the t-channel, such as DIS, VBF and VBS. The latter two processes are handled following a factorised approach, i.e. neglecting non-factorisable corrections between the two hadronic sectors. The main novelty of these showers, with respect to the PanScales showers for hadron collisions introduced in Refs. [43, 44], is that

the transverse-momentum recoil due to initial-state radiation is smoothly redistributed primarily to partons in the current hemisphere (i.e. anti-parallel to the direction of the incoming proton in the Breit frame). This feature ensures that partons in the remnant hemisphere remain mostly unaffected, which is required from colour coherence. Furthermore, compared to standard showers for DIS and VBF/VBS, our showers differ in the choice of the dipole partitioning: this is not done in the dipole frame, but in the Breit frame. This, combined with a global recoil scheme or with a careful choice of the ordering scale, prevents soft gluons from taking unphysical recoil.

We have carried out a number of fixed-order tests, focusing on DIS, such as analysing the phase-space contours for two emissions with commensurate softness (Section 4.1), and colour/spin matrix-element comparisons (Section 4.2 and Appendix F), related to the PanScales conditions needed to achieve NLL accuracy. All-order validations of our new showers for DIS have also been carried out for a variety of observables. These include tests of the DGLAP evolution (Section 5.1), jet-multiplicity (Section 5.2), DIS continuously-global event-shapes (Section 5.3), and the scalar sum of transverse momenta in a fixed rapidity slice (Section 5.4). In our comparisons, we introduced new continously-global event shapes, which rely on the use of Lund Plane coordinates and a jet algorithm specific for DIS. All these tests were carried out including subleading colour corrections, except for those of the non-global observable. The PanLocal shower with $\beta_{\mathrm{PS}} = 0.5$ and PanGlobal showers with $\beta_{\mathrm{PS}} = 0, 0.5$ sucessfully pass the fixed- and all-order NLL accuracy tests. We have compared these showers to a 'standard' transverse-momentum ordered shower, Dipole-k_t, which has fully local transverse-momentum recoil. Differences between the LL-accurate Dipole-k_t and the new NLL-accurate showers can grow up to 15% for phenomenologically relevant continuously-global event-shape observables such as the current-hemisphere broadening.[11] The SL accuracy of our showers established for DIS processes, automatically propagates to VBF/VBS processes in the factorised approach. This is the first time such accuracy is achieved for VBF/VBS global and non-global observables. The neglected non-factorisable contributions are SL subleading colour corrections, and are typically further surpressed after applying VBF cuts.

In Section 6 we present an exploritory phenomenological application of our newly developed showers for Higgs production in VBF at $\sqrt{s} = 13.6$ TeV. For each of the two hadronic sectors individually, we choose separate values for the shower starting, renormalisation, and factorisation scales. While we examined the impact of variations in the renormalisation and factorisation scales, it is important to note that such variations typically do not capture all sources of uncertainty. Indeed, the fact that we have developed not one, but several showers, is important for a realistic estimate of shower uncertainties, as the spread of predicitions obtained with our PanScales showers is not captured by the scale uncertainty. For inclusive observables, the LL shower is contained in the spread of our newly-developed NLL ones. However, for exclusive observables, like the rapidity or transverse momentum of the third jet, we find that the Dipole-k_t predictions typically overshoot the NLL showers.

---

[11] The NLL test for the Dipole-k_t shower has been performed implementing subleading colour corrections with the NODS colour scheme, despite the fact that the colour-factor-from-emitter scheme is the standard choice for such showers.

This discrepancy can be attributed to the fact that the Dipole-k_t shower typically produces a higher rate of 3-jet events compared to our NLL showers. Next steps involve matching the NLL-accurate showers to the NLO fixed-order results, where care needs to be taken not to compromise the NLL accuracy [74], as well as including heavy-quark mass effects to handle t-channel single-top production.

Acknowledgements

A   Description of the momentum-conservation restoring boost

This appendix details the derivation of the boost $\Lambda^{\mu\nu}$, introduced in Sec. 3.2. For PanGlobal this boost acts on the collection of final-state partons $\bar{p}_X^\mu$ to restore momentum conservation. For the PanLocal shower it in addition also acts on the incoming parton $\bar{p}_1^\mu$ to restore momentum conservation after the collection of partons are rotated so that $\bar{p}_1^\mu$ is aligned with the direction of n_1^μ. We demand that the boost preserves the invariant mass of $\bar{p}_X^\mu$, which implies

$$\Lambda^{\mu\nu}\left(\bar{p}_{X,\nu}\right) \equiv p_X^\mu = n_2^\mu + \frac{\bar{p}_X^2}{Q^2}n_2^\mu. \tag{A.1}$$

Using a Sudakov decomposition of $\bar{p}_X$ along the directions of n_1^μ and n_2^μ, eq. (A.1) can be written as

$$\Lambda^{\mu\nu}\left(\beta n_{2,\nu} + \frac{\bar{p}_X^2 + p_t^2}{\beta Q^2}n_{1,\nu} + p_{\perp,\nu}\right) = n_2^\mu + \frac{\bar{p}_X^2}{Q^2}n_1^\mu, \tag{A.2}$$

with $p_\perp^2 = -p_t^2 < 0$, $n_1^2 = n_2^2 = 0$, $2n_1 \cdot n_2 = Q^2$ and $p_\perp \cdot n_{1,2} = 0$. We aim to design a boost that acts as a rescaling for momentum components along n_1^μ, and assigns all the transverse momentum recoil to the n_2^μ direction.[12] Inverting eq. (A.2), we have

$$\left[\Lambda^{-1}\right]^{\mu\nu}\left(n_{2,\nu} + \frac{\bar{p}_X^2}{Q^2}n_{1,\nu}\right) = \beta n_2^\mu + \frac{\bar{p}_X^2 + p_t^2}{\beta Q^2}n_1^\mu + p_\perp^\mu. \tag{A.3}$$

---

[12]The construction of this boost shares similarities with the boost used in Deductor for $pp \to Z/h$ collisions [45].

We now may examine the action of the inverse boost on the n_1^μ and n_2^μ components individually. The direction n_2^μ absorbs all the transverse-momentum recoil, but also must stay massless, meaning it also must absorb a component in the n_1^μ direction. To satisfy these constraints we infer that

$$\left[\Lambda^{-1}\right]^{\mu\nu} n_{2,\nu} \equiv \beta n_2^\mu + \frac{p_t^2}{\beta Q^2} n_1^\mu + p_\perp^\mu \,. \tag{A.4}$$

To satisfy eq. (A.3) we then have to require

$$\left[\Lambda^{-1}\right]^{\mu\nu} n_{1,\nu} \equiv \frac{Q^2}{\bar{p}_X^2} \left(\beta n_2^\mu + \frac{\bar{p}_X^2 + p_t^2}{\beta Q^2} n_1^\mu + p_\perp^\mu - \left[\Lambda^{-1}\right]^{\mu\nu} n_{2,\nu} \right) = \frac{1}{\beta} n_1^\mu \,. \tag{A.5}$$

We now have established the action of the inverse boost on the n_1^μ and n_2^μ directions. What remains is to determine what happens when the inverse boost acts on a generic transverse-momentum component $q_\perp^\mu$ (with $q_\perp \cdot n_{1,2} = 0$). We require that the action of the inverse boost on such a perpendicular component is only allowed to bring in a component in the direction of n_1^μ. Furthermore, the perpendicular component does not get rescaled, so that its norm is preserved:

$$\left[\Lambda^{-1}\right]^{\mu\nu} q_{\perp,\nu} = q_\perp^\mu + A n_1^\mu \,. \tag{A.6}$$

To find the value of A, we require that the invariant mass of generic vector $q^\mu = a_q n_1^\mu + b_q n_2^\mu + q_\perp^\mu$ is preserved by the boost. This leads to

$$A = -\frac{2q_\perp \cdot p_\perp}{\beta Q^2} \,. \tag{A.7}$$

Note that we cannot introduce a component along n_2^μ in the action of the inverse boost on a transverse component. To see this, consider the action of the inverse boost on a generic transverse component $q_\perp^\mu$ where we now assign a n_2^μ component,

$$\left[\Lambda^{-1}\right]^{\mu\nu} q_{\perp,\nu} = B n_2^\mu + q_\perp^\mu \,. \tag{A.8}$$

With this definition, the action of the inverse boost on a generic four-momentum q^μ would become

$$\left[\Lambda^{-1}\right]^{\mu\nu} q_\nu = \left(\frac{a_q}{\beta} + \frac{b_q\, p_t^2}{\beta Q^2} \right) n_1^\mu + \left(b_q \beta + B \right) n_2^\mu + b_q p_\perp^\mu + q_\perp^\mu \,. \tag{A.9}$$

Requiring that the boost leaves the invariant mass of q^μ unchanged gives us

$$B = \frac{2 p_\perp \cdot q_\perp}{a_q Q^2 + b_q p_t^2} b_q \beta \,. \tag{A.10}$$

This is not linear in q^μ, which means that if we would consider $l^\mu = q^\mu + q'^\mu$, we would have $\left[\Lambda^{-1}\right]^{\mu\nu} l_\nu \neq \left[\Lambda^{-1}\right]^{\mu\nu} q_\nu + \left[\Lambda^{-1}\right]^{\mu\nu} q'_\nu$. Therefore, B needs to be set to zero.

The action of $\left[\Lambda^{-1}\right]^{\mu\nu}$ is now fully specified, and we can invert it to find $\Lambda^{\mu\nu}$. We then obtain

$$\Lambda^{\mu\nu} n_{1,\nu} = \beta\, n_1^\mu \,, \tag{A.11a}$$

$$\Lambda^{\mu\nu}q_{\perp,\nu} = q_\perp^\mu + \frac{2q_\perp \cdot p_\perp}{Q^2}n_1^\mu\,, \tag{A.11b}$$

$$\Lambda^{\mu\nu}n_{2,\nu} = \frac{1}{\beta}\left(n_2^\mu + \frac{p_t^2}{Q^2}n_1^\mu - p_\perp^\mu\right)\,, \tag{A.11c}$$

so that the final form of the boost reads

$$\Lambda^{\mu\nu} = g^{\mu\nu} + \frac{2n_1^\mu}{Q^2}\left[(\beta - 1)n_2^\nu + \frac{p_t^2}{\beta Q^2}n_1^\nu + p_\perp^\nu\right] + \frac{2n_2^\mu n_1^\nu}{Q^2}\frac{1-\beta}{\beta} - \frac{2p_\perp^\mu n_1^\nu}{\beta Q^2}\,. \tag{A.12}$$

B   Local rescaling factors for PanGlobal

In this section we derive the rescaling factors r_{L} appearing in the PanGlobal map of eq. (3.15), distiguishing between final-final and initial-final dipoles. We also comment on the implementation for hadron-hadron colliders, which also contains initial-initial dipoles.

B.1   Final-final dipoles

For an emission off a final-final dipole we have,

$$\bar{p}_i^\mu = r_{\text{L}}(1 - a_k)\tilde{p}_i^\mu\,, \tag{B.1a}$$

$$\bar{p}_j^\mu = r_{\text{L}}(1 - b_k)\tilde{p}_j^\mu\,, \tag{B.1b}$$

$$\bar{p}_k^\mu = r_{\text{L}}(a_k\tilde{p}_i^\mu + b_k\tilde{p}_k^\mu + k_\perp^\mu)\,, \tag{B.1c}$$

and hence the final-state partonic momentum now reads

$$\bar{p}_X^\mu = \tilde{p}_X^\mu + p_i^\mu + p_j^\mu + p_k^\mu - \tilde{p}_i^\mu - \tilde{p}_j^\mu = \tilde{p}_X^\mu + (r_{\text{L}} - 1)(\tilde{p}_i^\mu + \tilde{p}_j^\mu) + r_{\text{L}}k_\perp^\mu. \tag{B.2}$$

As discussed in Ref. [72], when $\tilde{p}_i^\mu$ and $\tilde{p}_j^\mu$ are close in angle, $k_\perp \cdot Q$ can be large, despite $k_\perp^2$ being small. Practically for our DIS map, this means that when $k_\perp^\mu$ carries a large component aligned along the x or y axis, or along n_2^μ, the boost applied to the collection of the final-state partons is substantial, while when $k_\perp^\mu$ carries a large component along n_1^μ, we need to introduce a large rescaling for the intial-state parton. In all of these cases, we would produce undesired correlations with other partons in the event, that we prevent by adopting the energy-preserving solution proposed by Ref. [72]. In particular, in this case we impose that $\bar{p}_X \cdot Q = \tilde{p}_X \cdot Q$, leading to

$$r_{\text{L}} = \frac{(\tilde{p}_i + \tilde{p}_j) \cdot Q}{(\tilde{p}_i + \tilde{p}_j + k_\perp) \cdot Q} = \frac{\tilde{s}_i + \tilde{s}_j}{\tilde{s}_i + \tilde{s}_j + 2k_\perp \cdot Q}. \tag{B.3}$$

This guarantees that all the components of the momentum imbalance due to the map, i.e.

$$\bar{p}_X^\mu - q_{\text{DIS}}^\mu - \tilde{p}_1^\mu = \bar{p}_X^\mu - \tilde{p}_X^\mu = (r_{\text{L}} - 1)(\tilde{p}_i^\mu + \tilde{p}_j^\mu) + r_{\text{L}}k_\perp^\mu, \tag{B.4}$$

are proportional to $|k_\perp|$ (or $|k_\perp|^2$), and hence are small not only when a_k are b_k small, but also when $\tilde{s}_{ij}$ is small, i.e. in the triple-collinear limit.

B.2 Initial-final dipoles

For an initial-final dipole, we have

$$\bar{p}_i^\mu = r_{\rm L}(1 + a_k)\tilde{p}_i^\mu \,, \tag{B.5}$$

$$\bar{p}_j^\mu = r_{\rm L}(1 - b_k)\tilde{p}_j^\mu \,, \tag{B.6}$$

$$\bar{p}_k^\mu = r_{\rm L}(a_k\tilde{p}_i^\mu + b_k\tilde{p}_k^\mu + k_\perp^\mu) \,. \tag{B.7}$$

We now will proof that we may safely set $r_{\rm L} = 1$, and do not encounter the issue in the triple-collinear configuration that arises for FF dipoles. Using $\tilde{s}_i = 2\tilde{p}_i \cdot Q = M_X^2 + Q^2$, the partonic final-state momentum after the mapping becomes

$$\bar{p}_X^\mu = \tilde{p}_X^\mu - \tilde{p}_j^\mu + p_j^\mu + p_k^\mu = \frac{\tilde{s}_i(1 + a_k r_{\rm L}) - Q^2}{Q^2}n_1^\mu + n_2^\mu + r_{\rm L}k_\perp^\mu + (r_{\rm L} - 1)\tilde{p}_j^\mu. \tag{B.8}$$

We now aim to write Eq. (B.8) in terms of n_1^μ, n_2^μ and a perpendicular component. To this end, parameterising the momenta in the DIS frame, we write

$$\tilde{p}_i^\mu = \frac{\tilde{s}_i}{2Q}(0, 0, -1; 1) = \frac{\tilde{s}_i}{Q^2}n_1^\mu \,, \tag{B.9}$$

$$\tilde{p}_j^\mu = \frac{\tilde{s}_j}{2Q}(\sin\theta_{ij}\sin\phi_j, \sin\theta_{ij}\cos\phi_j, -\cos\theta_{ij}; 1) \tag{B.10}$$

$$= \frac{\tilde{s}_j(1 + \cos\theta_{ij})}{2Q^2}n_1^\mu + \frac{\tilde{s}_j(1 - \cos\theta_{ij})}{2Q^2}n_2^\mu + p_{j,\perp}^\mu \,,$$

with

$$p_{j,\perp}^\mu = \frac{\tilde{s}_j\sin\theta_{ij}}{2Q}(\sin\phi_j, \cos\phi_j, 0; 0) \,. \tag{B.11}$$

The vectors

$$\hat{k}_{\perp,1}^\mu = (\cos\phi_j, -\sin\phi_j, 0, 0) \,, \quad \hat{k}_{\perp,2}^\mu = \left(\sin\phi_j, \cos\phi_j, -\frac{\sin\theta_{ij}}{1 - \cos\theta_{ij}}; \frac{\sin\theta_{ij}}{1 - \cos\theta_{ij}}\right), \tag{B.12}$$

form a basis of space-like vectors with norm -1, orthogonal to $\tilde{p}_i^\mu$ and $\tilde{p}_j^\mu$, and we define

$$k_\perp^\mu = k_t(\hat{k}_{\perp,1}^\mu\sin\phi_k + \hat{k}_{\perp,2}^\mu\cos\phi_k), \tag{B.13}$$

with $k_t = \sqrt{a_k b_k \tilde{s}_{ij}}$. Note that $\hat{k}_{\perp,1}^\mu$ is orthogonal to both n_1^μ and n_2^μ, while $\hat{k}_{\perp,2}^\mu$ carries a longitudinal component. To extract this longitudinal piece, we further decompose

$$\hat{k}_{\perp,2}^\mu = \hat{k}_{\perp,2}^{\prime\mu} + \frac{2\sin\theta_{ij}}{Q(1 - \cos\theta_{ij})}n_1^\mu, \text{ with } \hat{k}_{\perp,2}^{\prime\mu} = (\sin\phi_j, \cos\phi_j, 0; 0) = \frac{p_{j,\perp}^\mu}{\sqrt{-p_{j,\perp}^2}} \,, \tag{B.14}$$

where $\hat{k}_{\perp,2}^{\prime\mu}$ is now orthogonal to both n_1^μ and n_2^μ. We then write

$$r_{\rm L}k_\perp^\mu + (r_{\rm L} - 1)\tilde{p}_j^\mu = \Delta\alpha\,n_1^\mu + \Delta\beta\,n_2^\mu + p_\perp^\mu, \tag{B.15}$$

with

$$\Delta\alpha = \frac{(r_{\rm L} - 1)\tilde{s}_{ij}(1 + \cos\theta_{ij})}{2Q^2} + \frac{2r_{\rm L}k_t\sin\theta_{ij}\cos\phi_k}{Q(1 - \cos\theta_{ij})} \,, \tag{B.16}$$

$$\Delta\beta = \frac{(r_{\mathrm{L}} - 1)\tilde{s}_{ij}(1 - \cos\theta_{ij})}{2Q^2}\,, \tag{B.17}$$

$$p_\perp^\mu = r_{\mathrm{L}} k_t \sin\phi_k \hat{k}_{\perp,1}^\mu + \left[(r_{\mathrm{L}} - 1)\frac{\tilde{s}_j \sin\theta_{ij}}{2Q} + r_{\mathrm{L}} k_t \cos\phi_k\right]\hat{k}_{\perp,2}^{\prime,\mu}\,, \tag{B.18}$$

so that

$$\bar{p}_X^\mu = \frac{\bar{p}_X^2 + p_t^2}{(1 + \Delta\beta)Q^2}n_1^\mu + (1 + \Delta\beta)n_2^\mu + p_\perp^\mu\,, \tag{B.19}$$

with $p_t^2 = -p_\perp^2$. For $\theta_{ij} \to 0$, i.e. in the triple-collinear limit, we note that $\Delta\beta \to 0$ and $p_t \to 0$, thus $\bar{p}_X^\mu \approx \frac{\bar{p}_X^2}{Q^2}n_1^\mu + n_2^\mu$. The action of the momentum-conserving boost is therefore minimal, as it needs to act on $\bar{p}_X^\mu$ such that $\Lambda^\mu{}_\nu\bar{p}_X^\nu = \frac{\bar{p}_X^2}{Q^2}n_1^\mu + n_2^\mu \simeq \bar{p}_X^\mu$. In other words, we can safely use $r_{\mathrm{L}} = 1$ without introducing any long-distance correlations. Indeed, for $r_{\mathrm{L}} = 1$ we simply obtain for the momentum imbalance after the mapping

$$\bar{p}_X^\mu - q_{\mathrm{DIS}}^\mu - \bar{p}_i^\mu = \frac{2k_t \sin\theta_{ij}}{Q(1 - \cos\theta_{ij})}n_1^\mu + k_t(\hat{k}_{\perp,1}^\mu \sin\phi_k + \hat{k}_{\perp,2}^{\prime,\mu}\cos\phi_k)\,. \tag{B.20}$$

In the triple-collinear limit this becomes

$$\bar{p}_X^\mu - q_{\mathrm{DIS}}^\mu - \bar{p}_i^\mu \approx \frac{4}{Q^2}\sqrt{a_k b_k \tilde{s}_i \tilde{s}_j}\,\mathrm{Sign}(\theta_{ij})n_1^\mu + \mathcal{O}(\theta_{ij})\,. \tag{B.21}$$

This four-vector is aligned along n_1^μ, and the imbalance is reabsorbed locally within the dipole by rescaling $\bar{p}_i$, without affecting any other partons.

B.3 Initial-initial dipoles and extention to hadron-hadron colliders

The PanGlobal shower for hadron collisions of Refs. [43, 44] features the same issues as the previously discussed DIS variant, and the final-state variant presented in Ref. [38]. For the pp variant, the transverse-momentum imbalance is fully absorbed by the hard system (which coincides with the colour singlet in Ref. [43]), while the two initial-state partons are rescaled to ensure that the invariant mass of this system is unchanged. It is straightforward to show that for initial-initial dipoles, we do not need to modify the original proposal, as no triple-collinear configuration can arise, since the two initial-state particles are never close in angle. Like for DIS, for emissions off initial-final dipoles, the longitudinal rescaling ensures that in the triple-collinear limit no parton, besides the initial-state one contained in the emitting dipole, is subject to modifications, thereby enabling us to use once again the original map. However, for final-final dipoles, we need to introduce a local rescaling r_{L}, as the triple-collinear configuration can result in a substantial modification to the hard system. For these types of emissions, we employ the definition of the rescaling given in eq. (B.3), where now Q^μ represents the momentum of the hard system. The rescaling and boost procedure then follows that detailed in Ref. [43]. The modifications presented here do not alter the logarithmic accuracy of the shower.

C Cambridge/Aachen algorithm for DIS and Lund variables

In this section, we describe the exclusive Cambridge/Aachen algorithm for DIS. The e^+e^- variant was introduced in Ref. [102], while a DIS variant was proposed in Ref. [103]. This

algorithm is similar to the $k_\perp$ algorithm for DIS introduced of Ref. [102], but using an angular distance to determine the cluster sequence.

Conversely to the original proposal, here we do not employ a resolution variable (or equivalently, we set $y_{\rm cut} = 0$). Instead, the clustering procedure we use is

- For every final-state parton i, define the angular distance with respect to the beam B

$$d_{iB} = 1 - \cos\theta_i \,, \tag{C.1}$$

  where θ_i is the angle between i and B in the Breit frame. In addition, define the angular distance between each pair of partons i and j, again in the Breit frame,

$$d_{ij} = 1 - \cos\theta_{ij} \,. \tag{C.2}$$

- Find the smallest distance among $\{d_{iB}, d_{ij}\}$. If it is of the type d_{iB}, we remove i from the list of partons, and make it a candidate jet. If instead it is of the type d_{ij}, we remove i and j from the list, and insert a new pseudo-parton with total momentum $p_i^\mu + p_j^\mu$.

- Repeat the procedure until only one pseudo-parton remains in the list: this pseudo-parton forms its own candidate jet.

We have now a list of candidate jets, among which we need to find the final-state macro jet, which contains all the radiation from the original final-state quark that had a momentum n_2^μ. Each jet momentum p_j^μ can be written as

$$p_j^\mu = \alpha_j P^\mu + \beta_j n_2^\mu + p_{\perp,j}^\mu \,, \tag{C.3}$$

where P^μ is the incoming proton momentum. We label as final-state macro jet the one with the largest β_j value, i.e. the one that retains the largest fraction of the light-cone component of the original final-state quark in the Breit frame. This jet can easily be found by searching for the jet whose momentum p_j^μ yields the largest value of $p_j \cdot P$.

After this clustering algorithm, the event contains a collection of initial-state/beam jets and one final-state macro jet. To calculate our event shapes we need to define the primary Lund-plane variables. For each initial-state/beam jet, we define the primary Lund-plane coordinates as

$$\eta_i = -\frac{1}{2} \ln \frac{1 - \cos\theta_i}{1 + \cos\theta_i} \,, \qquad k_{t,i} = E_i \sin\theta_i \,. \tag{C.4}$$

Note that these exactly correspond to the pseudorapidity and transverse-momentum of i in the Breit frame. The negative sign of the pseudorapidity is due to the convention to orientate the incoming beam along the negative z axis in the Breit frame.

For the final-state macro jet a different procedure is adopted. We consider the clustering sequence starting from the last recombination, and consider the energies of the two pseudo-jets that were combined, E_i and E_j, where $E_i > E_j$. The softer pseudojet, which we have labelled with j, is then promoted to be a jet, with Lund coordinates

$$\eta_j = \frac{1}{2} \ln \frac{1 - \cos\theta_{ij}}{1 + \cos\theta_{ij}} \,, \quad k_{t,j} = E_j \sin\theta_{ij} \,. \tag{C.5}$$

We iterate this procedure for the most energetic pseudojet.

The procedure is terminated when the most-energetic pseudojet has no further children, i.e. it is a single parton (notice that this parton is not associated with any jet). The secondary Lund plane is defined by the jet (found inside the final-state macrojet, or among the collection of initial-state jets) that has the largest value for the Lund variable k_t.

D   Resummation formulae for continuously-global observables

We consider a continuously-global observable [87] that in the soft-collinear limit behaves as

$$O \sim \frac{p_T}{Q} e^{-\beta_{\mathrm{obs}}|\eta|}. \tag{D.1}$$

The cumulative cross section at NLL accuracy can be written as

$$\Sigma_{\mathrm{NLL}}(O < e^L) = \exp\left[-L g_1(\bar{\lambda}) + g_2(\bar{\lambda})\right], \tag{D.2}$$

with $\bar{\lambda} = -\alpha_s b_0 L$ (and $L < 0$) and

$$b_0 = \frac{11 C_A - 4 n_f T_R}{12\pi}. \tag{D.3}$$

The g_1 function contains the LL terms. For processes with two hard legs it reads

$$g_1^{\beta_{\mathrm{obs}}=0} = \frac{C_i}{\pi b_0 \bar{\lambda}} \left(2\bar{\lambda} + \ln(1 - 2\bar{\lambda})\right), \tag{D.4a}$$

$$g_1^{\beta_{\mathrm{obs}}\neq0} = \frac{C_i}{\pi b_0 \bar{\lambda}\beta_{\mathrm{obs}}} \left((1 + \beta_{\mathrm{obs}} - 2\bar{\lambda}) \ln\left(1 - \frac{2\bar{\lambda}}{1 + \beta_{\mathrm{obs}}}\right) - (1 - 2\bar{\lambda})\ln(1 - 2\bar{\lambda})\right), \tag{D.4b}$$

where C_i is the Casimir factor ($C_i = C_F$ for quark radiators, C_A for gluon radiators). The NLL term g_2 can be written as

$$g_2^{\beta_{\mathrm{obs}}} = \ln \frac{f_i\left(x_{\mathrm{DIS}}, Q^2 e^{2L/(1+\beta_{\mathrm{obs}})}\right)}{f_i\left(x_{\mathrm{DIS}}, Q^2\right)} + \bar{g}_2^{\beta_{\mathrm{obs}}} + \ln \mathcal{F}_{\mathrm{obs}}, \tag{D.5}$$

where f_i is the PDF of the incoming parton. We use $\bar{g}_2^{\beta_{\mathrm{obs}}}$ to denote the universal β_{obs}-dependent term originating from soft and hard-collinear emissions, and $\mathcal{F}_{\mathrm{obs}}$ is an observable-dependent correction. We have

$$\bar{g}_2^{\beta_{\mathrm{obs}}=0} = \frac{C_i}{\pi b_0^2} \left[b_0 B_i^{(1)} \ln(1 - 2\bar{\lambda}) - \frac{K}{2\pi} \left(\frac{2\bar{\lambda}}{1 - 2\bar{\lambda}} + \ln(1 - 2\bar{\lambda}) \right) \right. \tag{D.6a}$$

$$\left. + \frac{b_1}{b_0} \left(\frac{2\bar{\lambda} + \ln(1 - 2\bar{\lambda})}{1 - 2\bar{\lambda}} + \frac{1}{2} \ln^2(1 - 2\bar{\lambda}) \right) \right],$$

$$\bar{g}_2^{\beta_{\mathrm{obs}}\neq0} = \frac{C_i}{\pi b_0^2 \beta_{\mathrm{obs}}} \left[\frac{K}{2\pi} \left(\ln(1 - 2\bar{\lambda}) - (1 + \beta_{\mathrm{obs}}) \ln\left(1 - \frac{2\bar{\lambda}}{1 + \beta_{\mathrm{obs}}}\right) \right) \right. \tag{D.6b}$$

$$\left. + b_0 \beta_{\mathrm{obs}} B_i^{(1)} \ln\left(1 - \frac{2\bar{\lambda}}{1 + \beta_{\mathrm{obs}}}\right) - \frac{b_1}{b_0} \left(\frac{1}{2} \ln^2(1 - 2\bar{\lambda}) + \ln(1 - 2\bar{\lambda}) \right. \right.$$

$$- \frac{1}{2}(1 + \beta_{\mathrm{obs}}) \ln^2 \left(1 - \frac{2\bar\lambda}{1 + \beta_{\mathrm{obs}}} \right) - (1 + \beta_{\mathrm{obs}}) \ln \left(1 - \frac{2\bar\lambda}{1 + \beta_{\mathrm{obs}}} \right) \Bigg) \Bigg],$$

with

$$b_1 = \frac{17 C_A^2 - 10 C_A n_f T_R - 6 C_F n_f T_R}{24\pi^2}, \qquad K = \left(\frac{67}{18} - \frac{\pi^2}{6} \right) C_A - \frac{10}{9} n_f T_R, \qquad \text{(D.7)}$$

$$B_q^{(1)} = -\frac{3}{4}, \quad B_g^{(1)} = \frac{-11 C_A + 4 n_F T_R}{12 C_A}.$$

Finally, we come to the observable-dependent correction. For the max-type observable $M_{j, \beta_{\mathrm{obs}}}$ (defined in eq. (5.10)), we have $\ln \mathcal{F}_{\mathrm{obs}} = 0$, while for $S_{p/j, \beta_{\mathrm{obs}}}$, (eq. (5.10)), this correction reads

$$\ln \mathcal{F}_{S_j, \beta_{\mathrm{obs}}} = -\gamma_E R'(\bar\lambda) - \ln \Gamma \left(1 + R'(\bar\lambda) \right), \qquad \text{(D.8)}$$

with $R'(\bar\lambda)$ defined as $\partial_L \left(L g_1(\bar\lambda) \right)$,

$$R'_{\beta_{\mathrm{obs}}=0}(\bar\lambda) = \frac{4 C_i}{\pi b_0} \frac{\bar\lambda}{1 - 2\bar\lambda}, \qquad \text{(D.9a)}$$

$$R'_{\beta_{\mathrm{obs}}\neq 0}(\bar\lambda) = \frac{2 C_i}{\pi b_0 \beta_{\mathrm{obs}}} \left[\ln \left(1 - \frac{2\bar\lambda}{1 + \beta_{\mathrm{obs}}} \right) - \ln(1 - 2\bar\lambda) \right]. \qquad \text{(D.9b)}$$

In Sec. 5.3 we also considered standard DIS event shapes, that have the property of being continuously global, and can be defined considering only partons in the current hemisphere: the thrust with respect to the photon axis and normalised to $Q/2$, τ_{zQ} (eq. (5.11c)), and the broadening with respect to the photon axis, normalised either to the energy in the current hemisphere B_{zE} (eq. (5.11a)) or to Q, B_{zQ} (eq. (5.11b)). The NLL analytic predictions for τ_{zQ} were computed for the first time in Ref. [73], and they are identical to those for $S_{\beta_{\mathrm{obs}}=1}$. The two definitions of broadening B_{zE} and B_{zQ} are equivalent at NLL, and the analytic prediction can be read from Ref. [90] to read

$$\ln \Sigma(B_z < e^L) = -g_1^{\beta_{\mathrm{obs}}=0}(\bar\lambda) L + \bar{g}_2^{\beta_{\mathrm{obs}}=0}(\bar\lambda) + \ln \mathcal{F}_B(\bar\lambda) + \ln \frac{f_i \left(x_{\mathrm{DIS}}, Q^2 e^{2L} \right)}{f_i \left(x_{\mathrm{DIS}}, Q^2 \right)}, \qquad \text{(D.10)}$$
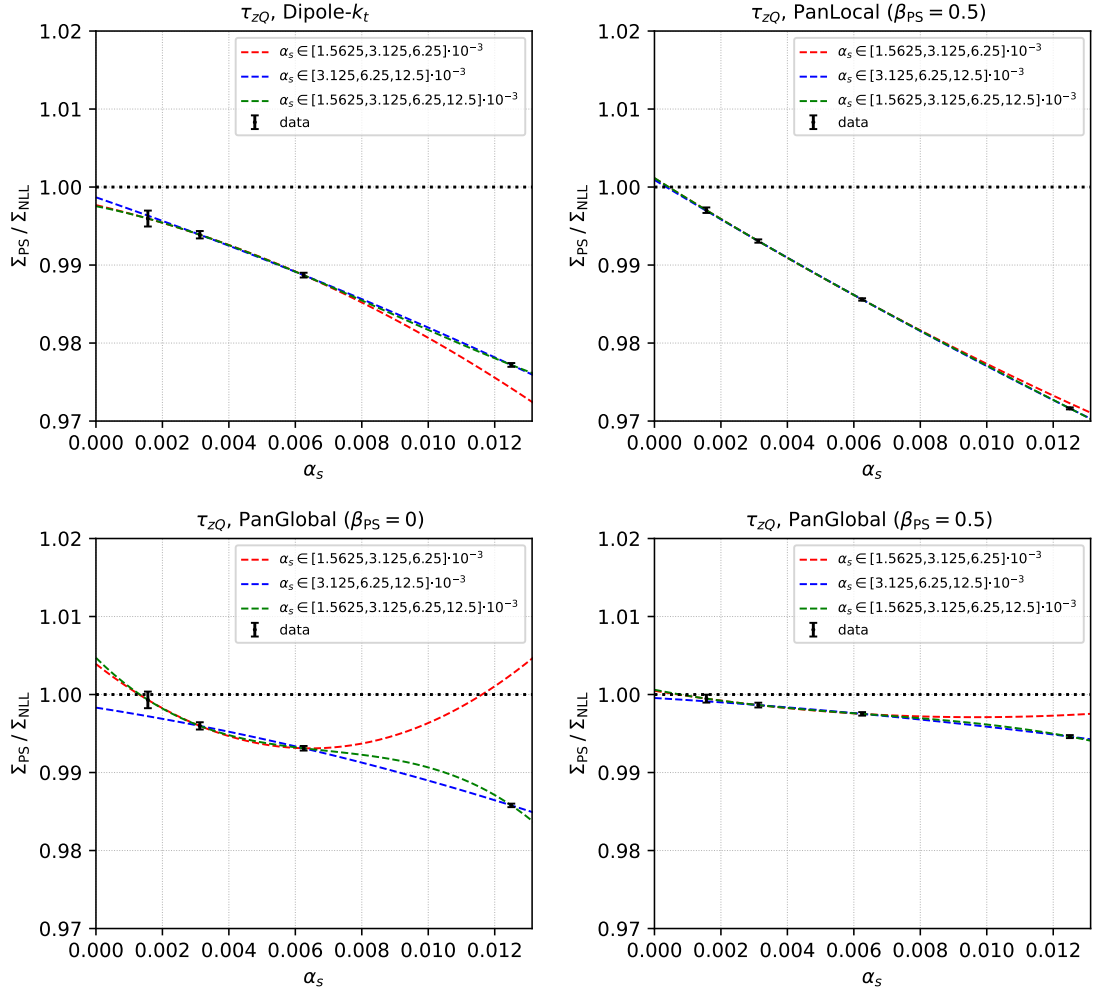
where B_z can be either B_{zE} or B_{zQ}. The observable-dependent factor $\ln \mathcal{F}_B$ had an analytic form that reads

$$\ln \mathcal{F}_B = -\frac{1}{2}(\ln 2 + 2\gamma_E) R' + \ln \Lambda(R') - \ln \Gamma(1 + R'), \qquad \text{(D.11a)}$$

$$\Lambda(R') = \int_0^\infty \frac{y \, dy}{(1 + y^2)^{3/2}} \left(\frac{y(1 + \sqrt{1 + y^2})}{8} \right)^{-R'/2}$$

$$= 8^{R'/2} \Gamma(1 - R'/4) \Gamma(1 + R') \frac{{}_2F_1(3R'/4, 1 + R', 2 + 3R'/4; -1)}{\Gamma(2 + 3R'/4)}, \qquad \text{(D.11b)}$$

where $R' = R'_{\beta_{\mathrm{obs}}=0}(\bar\lambda)$ defined in eq. (D.9a) and ${}_2F_1(a, b, c; z)$ is the hypergeometric function.

Figure 13: $\Sigma_{\mathrm{PS}}/\Sigma_{\mathrm{NLL}}$ for τ_{zQ} of eq. (5.11c) for Dipole-k_t (upper left), PanLocal($\beta_{\mathrm{PS}} = 0.5$) (upper right), PanGlobal($\beta_{\mathrm{PS}} = 0$) (lower left) and PanGlobal($\beta_{\mathrm{PS}} = 0.5$) (lower right) showers. The black dots represent the data (with the Monte Carlo error bars) obtained at α_s values of $0.0015625, 0.003125, 0.00625$ and 0.0125 with $\lambda = \alpha_s \ln \tau_{zQ} = -0.5$ held constant. The dashed curves show the interpolation of the data points, where red, blue and green represent the interpolation of the data at $\alpha_s \in [0.0015625, 0.003125, 0.00625]$, $\alpha_s \in [0.003125, 0.00625, 0.0125]$ and $\alpha_s \in [0.0015625, 0.003125, 0.00625, 0.0125]$ respectively.

E The $\alpha_s \to 0$ extrapolation and size of subleading contributions

In this appendix, we show the $\alpha_s \to 0$ extrapolation for τ_{zQ} as specified in Eq. (5.11c). In Fig. 13, we show the results obtained for ratio between the shower result and the analytic NLL expectation for the cumulative distributions for the Dipole-k_t, PanLocal($\beta_{\mathrm{PS}} = 0.5$), PanGlobal($\beta_{\mathrm{PS}} = 0$) and PanGlobal($\beta_{\mathrm{PS}} = 0.5$) showers for $\lambda = \alpha_s \ln \tau_{zQ} = -0.5$. These results are obtained with four different values $\alpha_s \in [0.0015625, 0.003125, 0.00625, 0.0125]$. The size of subleading contributions and the stability of the extrapolation depends on both

the shower (as can be seen in Fig. 13) and the observable.

We then fit the results using a polynomial $f(\alpha_s) = \sum_{i=0}^{n} c_i \alpha^i$, with n the (variable) number of data points. The $\alpha_s \to 0$ extrapolation is obtained through the coefficient c_0, i.e. the point where the curves cross the y-axis. The slope of the curves near $\alpha_s = 0$ indicates the size of NNLL corrections generated by the showers. Our current numerical precison prevents us from getting their precise estimate, but in all cases we find a value of order 1, as is expected since $\lambda = \mathcal{O}(1)$.

F Spin correlations

Spin correlations must be included to reproduce the correct azimuthal structure of strongly angular-ordered collinear splittings. This can be achieved by for example using the Collins-Knowles algorithm [104–107], which was also recently applied to the PanScales final-state and initial-state showers [43, 108]. In Ref. [109] the algorithm was further improved to include for the first time the treatment of the dominant leading-colour soft azimuthal correlations. In this appendix, we show that the algorithm introduced in Ref. [43] can be applied straightforwardly to DIS.

We consider the shower effective matrix element for the production of two extra partons i and j, and compare the result against the analytic expectation as a function of the azimuthal angle $\Delta\psi_{ij}$ between the planes spanned by two emissions i and j. At $\mathcal{O}(\alpha_s^2)$, the differential cross section can be written as

$$\frac{d\sigma}{d\Delta\psi_{ij}} \propto a_0 \left(1 + \frac{a_2}{a_0}\cos(2\Delta\psi_{ij})\right) = a_0 \left(1 + A(z_i)B(z_j)\cos(2\Delta\psi_{ij})\right), \qquad \text{(F.1)}$$

where ψ_{ij} is the azimuthal difference between the plane defined by the primary and secondary splittings with light-cone momentum fraction z_i and z_j, respectively. The values of a_0 and a_2 depend on the type of branching, and are a function of z_i and z_j. In the absence of spin correlations, the ratio a_2/a_0 would be 0.

In Fig. 14 we illustrate the ratio a_2/a_0 across several values of z_1 and z_2 for collinear-splittings involving an intermediate gluon. In particular, in the left panel we show the case in which the first emission is a final-state gluon, that further branches into a $q\bar{q}$ pair. In the right panel we instead consider the backward evolution of the initial-state quark into an initial-state gluon (g_I), and then an emission of a final-state gluon very collinear to the incoming beam. We only show the predictions obtained with the PanGlobal($\beta_{\text{obs}} = 0$) shower, but identical results can be obtained by considering the other PanScales showers. The differences between the shower predictions and the analytic expectation were always smaller that 10^{-6}, confirming our implementation at fixed-order accuracy.

References

[1] M. Bahr et al., *Herwig++ Physics and Manual*, *Eur. Phys. J.* **C58** (2008) 639–707, [0803.0883].

[2] J. Bellm et al., *Herwig 7.2 release note*, *Eur. Phys. J. C* **80** (2020) 452, [1912.06509].
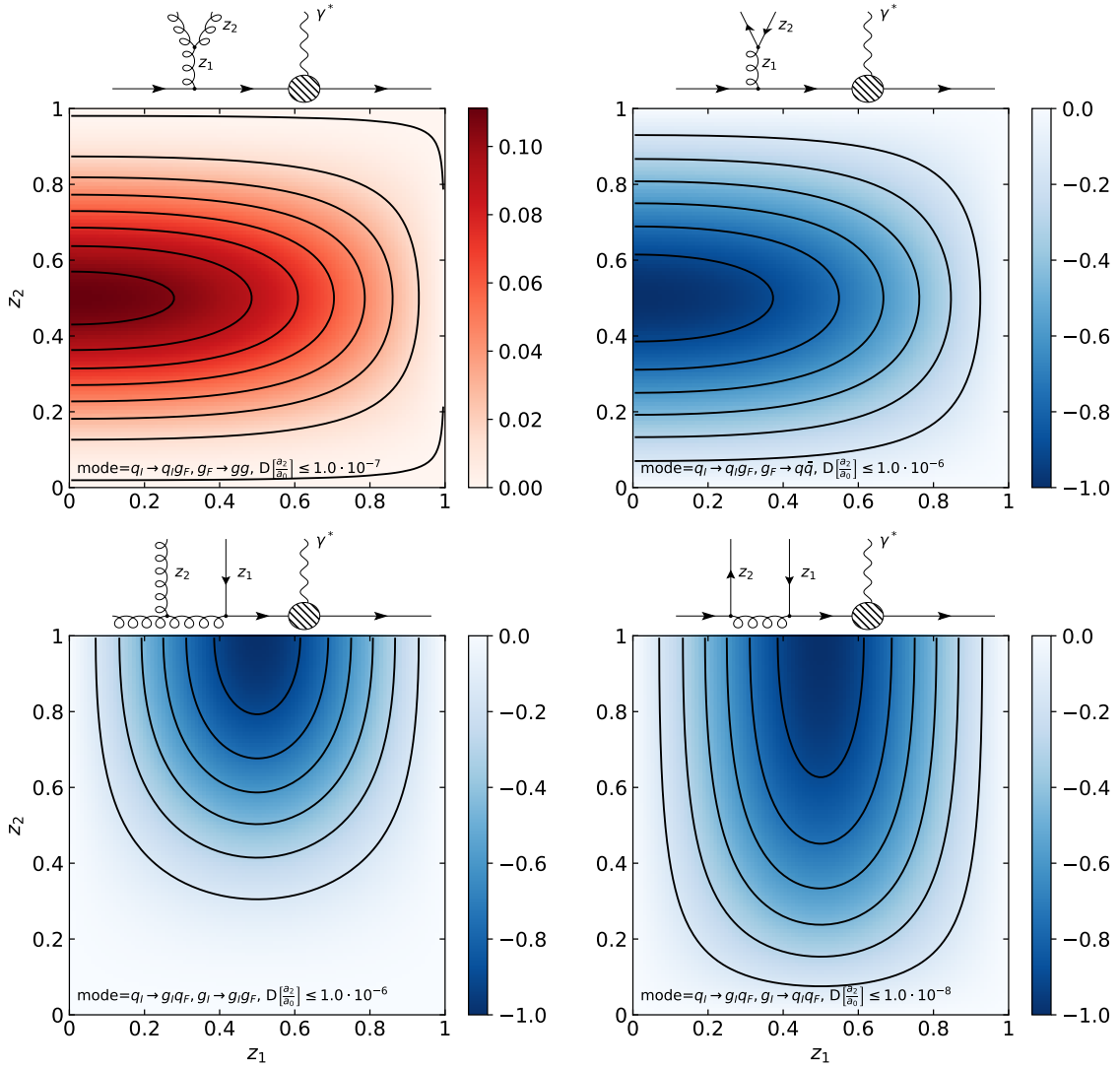
Figure 14: Size of the ratio between the two Fourier coefficients a_2/a_0, defined in eq. (F.1) at $\mathcal{O}(\alpha_s^2)$ for collinear splittings, for the PanGlobal($\beta_{\mathrm{obs}} = 0$) shower. The Feynman diagrams indicate the sequence of splittings under consideration. The black lines indicate constant values for this ratio, and are obtained using the analytic predictions. The (maximum) deviation of the analytic prediction and the shower is given by $\mathrm{D}\left[\frac{a_2}{a_0}\right] \leq \max\left|\left(\frac{a_2}{a_0}\right)_{\mathrm{PS}} - \left(\frac{a_2}{a_0}\right)_{\mathrm{ME}}\right|$, with $\left(\frac{a_2}{a_0}\right)_{\mathrm{PS}}$ the shower prediction and $\left(\frac{a_2}{a_0}\right)_{\mathrm{ME}}$ the analytic prediction for the matrix element.

[3] S. Gieseke, P. Stephens and B. Webber, *New formalism for QCD parton showers*, *JHEP* **12** (2003) 045, [hep-ph/0310083].

[4] G. Bewick, S. Ferrario Ravasio, P. Richardson and M. H. Seymour, *Logarithmic accuracy of angular-ordered parton showers*, *JHEP* **04** (2020) 019, [1904.11866].

[5] G. Bewick, S. Ferrario Ravasio, P. Richardson and M. H. Seymour, *Initial state radiation in*

the *Herwig 7 angular-ordered parton shower*, *JHEP* **01** (2022) 026, [2107.04051].

[6] A. Banfi, G. Corcella and M. Dasgupta, *Angular ordering and parton showers for non-global QCD observables*, *JHEP* **03** (2007) 050, [hep-ph/0612282].

[7] G. Gustafson and U. Pettersson, *Dipole Formulation of QCD Cascades*, *Nucl. Phys. B* **306** (1988) 746–758.

[8] S. Catani, F. Krauss, R. Kuhn and B. R. Webber, *QCD matrix elements + parton showers*, *JHEP* **11** (2001) 063, [hep-ph/0109231].

[9] F. Krauss, *Matrix elements and parton showers in hadronic interactions*, *JHEP* **08** (2002) 015, [hep-ph/0205283].

[10] N. Lavesson and L. Lonnblad, *Extending CKKW-merging to One-Loop Matrix Elements*, *JHEP* **12** (2008) 070, [0811.2912].

[11] S. Hoeche, F. Krauss, S. Schumann and F. Siegert, *QCD matrix elements and truncated showers*, *JHEP* **05** (2009) 053, [0903.1219].

[12] W. T. Giele, D. A. Kosower and P. Z. Skands, *Higher-Order Corrections to Timelike Jets*, *Phys. Rev. D* **84** (2011) 054003, [1102.2126].

[13] S. Plätzer, *Controlling inclusive cross sections in parton shower + matrix element merging*, *JHEP* **08** (2013) 114, [1211.5467].

[14] L. Lönnblad and S. Prestel, *Merging Multi-leg NLO Matrix Elements with Parton Showers*, *JHEP* **03** (2013) 166, [1211.7278].

[15] R. Frederix and S. Frixione, *Merging meets matching in MC@NLO*, *JHEP* **12** (2012) 061, [1209.6215].

[16] L. Lonnblad and S. Prestel, *Unitarising Matrix Element + Parton Shower merging*, *JHEP* **02** (2013) 094, [1211.4827].

[17] J. Bellm, S. Gieseke and S. Plätzer, *Merging NLO Multi-jet Calculations with Improved Unitarization*, *Eur. Phys. J. C* **78** (2018) 244, [1705.06700].

[18] H. Brooks and C. T. Preuss, *Efficient multi-jet merging with the Vincia sector shower*, *Comput. Phys. Commun.* **264** (2021) 107985, [2008.09468].

[19] K. Hamilton, P. Nason, C. Oleari and G. Zanderighi, *Merging H/W/Z + 0 and 1 jet at NLO with no merging scale: a path to parton shower + NNLO matching*, *JHEP* **05** (2013) 082, [1212.4504].

[20] S. Alioli, C. W. Bauer, C. Berggren, F. J. Tackmann, J. R. Walsh and S. Zuberi, *Matching Fully Differential NNLO Calculations and Parton Showers*, *JHEP* **06** (2014) 089, [1311.0286].

[21] S. Hoeche, Y. Li and S. Prestel, *Higgs-boson production through gluon fusion at NNLO QCD with parton showers*, *Phys. Rev.* **D90** (2014) 054011, [1407.3773].

[22] P. F. Monni, P. Nason, E. Re, M. Wiesemann and G. Zanderighi, *MiNNLO$_{PS}$: A new method to match NNLO QCD to parton showers*, 1908.06987.

[23] J. M. Campbell, S. Höche, H. T. Li, C. T. Preuss and P. Skands, *Towards NNLO+PS matching with sector showers*, *Phys. Lett. B* **836** (2023) 137614, [2108.07133].

[24] S. Prestel, *Matching N3LO QCD calculations to parton showers*, *JHEP* **11** (2021) 041, [2106.03206].

[25] M. L. Mangano, M. Moretti and R. Pittau, *Multijet matrix elements and shower evolution in hadronic collisions: $W b \bar{b} + n$ jets as a case study*, *Nucl. Phys.* **B632** (2002) 343–362, [hep-ph/0108069].

[26] K. Hamilton, P. Richardson and J. Tully, *A Modified CKKW matrix element merging approach to angular-ordered parton showers*, *JHEP* **11** (2009) 038, [0905.3072].

[27] A. B. Martinez, F. Hautmann and M. L. Mangano, *TMD evolution and multi-jet merging*, *Phys. Lett. B* **822** (2021) 136700, [2107.01224].

[28] S. Schumann and F. Krauss, *A Parton shower algorithm based on Catani-Seymour dipole factorisation*, *JHEP* **03** (2008) 038, [0709.1027].

[29] S. Platzer and S. Gieseke, *Coherent Parton Showers with Local Recoils*, *JHEP* **01** (2011) 024, [0909.5593].

[30] S. Hoeche and S. Prestel, *The midpoint between dipole and parton showers*, *Eur. Phys. J.* **C75** (2015) 461, [1506.05057].

[31] B. Cabouat and T. Sjöstrand, *Some Dipole Shower Studies*, *Eur. Phys. J.* **C78** (2018) 226, [1710.00391].

[32] H. Brooks, C. T. Preuss and P. Skands, *Sector Showers for Hadron Collisions*, *JHEP* **07** (2020) 032, [2003.00702].

[33] T. Sjostrand, S. Mrenna and P. Z. Skands, *PYTHIA 6.4 Physics and Manual*, *JHEP* **05** (2006) 026, [hep-ph/0603175].

[34] T. Sjöstrand, S. Ask, J. R. Christiansen, R. Corke, N. Desai, P. Ilten et al., *An Introduction to PYTHIA 8.2*, *Comput. Phys. Commun.* **191** (2015) 159–177, [1410.3012].

[35] T. Gleisberg, S. Hoeche, F. Krauss, M. Schonherr, S. Schumann, F. Siegert et al., *Event generation with SHERPA 1.1*, *JHEP* **02** (2009) 007, [0811.4622].

[36] SHERPA collaboration, E. Bothmann et al., *Event Generation with Sherpa 2.2*, *SciPost Phys.* **7** (2019) 034, [1905.09127].

[37] C. Bierlich et al., *A comprehensive guide to the physics and usage of PYTHIA 8.3*, 2203.11601.

[38] M. Dasgupta, F. A. Dreyer, K. Hamilton, P. F. Monni, G. P. Salam and G. Soyez, *Parton showers beyond leading logarithmic accuracy*, *Phys. Rev. Lett.* **125** (2020) 052002, [2002.11114].

[39] M. Dasgupta, F. A. Dreyer, K. Hamilton, P. F. Monni and G. P. Salam, *Logarithmic accuracy of parton showers: a fixed-order study*, *JHEP* **09** (2018) 033, [1805.09327].

[40] J. R. Forshaw, J. Holguin and S. Plätzer, *Building a consistent parton shower*, *JHEP* **09** (2020) 014, [2003.06400].

[41] Z. Nagy and D. E. Soper, *Summations by parton showers of large logarithms in electron-positron annihilation*, 2011.04777.

[42] F. Herren, S. Höche, F. Krauss, D. Reichelt and M. Schoenherr, *A new approach to color-coherent parton evolution*, 2208.06057.

[43] M. van Beekveld, S. Ferrario Ravasio, G. P. Salam, A. Soto-Ontoso, G. Soyez and R. Verheyen, *PanScales parton showers for hadron collisions: formulation and fixed-order studies*, *JHEP* **11** (2022) 019, [2205.02237].

[44] M. van Beekveld, S. Ferrario Ravasio, K. Hamilton, G. P. Salam, A. Soto-Ontoso, G. Soyez et al., *PanScales showers for hadron collisions: all-order validation*, *JHEP* **11** (2022) 020, [2207.09467].

[45] Z. Nagy and D. E. Soper, *On the transverse momentum in Z-boson production in a virtuality ordered parton shower*, *JHEP* **03** (2010) 097, [0912.4534].

[46] R. Covarelli, M. Pellen and M. Zaro, *Vector-Boson scattering at the LHC: Unraveling the electroweak sector*, *Int. J. Mod. Phys. A* **36** (2021) 2130009, [2102.10991].

[47] D. Buarque Franzosi et al., *Vector boson scattering processes: Status and prospects*, *Rev. Phys.* **8** (2022) 100071, [2106.01393].

[48] ATLAS collaboration, G. Aad et al., *A search for the dimuon decay of the Standard Model Higgs boson with the ATLAS detector*, *Phys. Lett. B* **812** (2021) 135980, [2007.07830].

[49] CMS collaboration, A. M. Sirunyan et al., *Evidence for Higgs boson decay to a pair of muons*, *JHEP* **01** (2021) 148, [2009.04363].

[50] CMS collaboration, *Measurements of Higgs boson production in the decay channel with a pair of τ leptons in proton-proton collisions at $\sqrt{s}$ = 13 TeV*, 2204.12957.

[51] ATLAS collaboration, G. Aad et al., *Measurements of Higgs boson production cross-sections in the $H \to \tau^+\tau^-$ decay channel in pp collisions at $\sqrt{s}$ = 13 TeV with the ATLAS detector*, *JHEP* **08** (2022) 175, [2201.08269].

[52] ATLAS collaboration, G. Aad et al., *Search for invisible Higgs-boson decays in events with vector-boson fusion signatures using 139 fb^{-1} of proton-proton data recorded by the ATLAS experiment*, *JHEP* **08** (2022) 104, [2202.07953].

[53] CMS collaboration, A. Tumasyan et al., *Search for invisible decays of the Higgs boson produced via vector boson fusion in proton-proton collisions at s=13 TeV*, *Phys. Rev. D* **105** (2022) 092007, [2201.11585].

[54] A. Ballestrero et al., *Precise predictions for same-sign W-boson scattering at the LHC*, *Eur. Phys. J. C* **78** (2018) 671, [1803.07943].

[55] B. Jäger, A. Karlberg, S. Plätzer, J. Scheller and M. Zaro, *Parton-shower effects in Higgs production via Vector-Boson Fusion*, *Eur. Phys. J. C* **80** (2020) 756, [2003.12435].

[56] S. Höche, S. Mrenna, S. Payne, C. T. Preuss and P. Skands, *A Study of QCD Radiation in VBF Higgs Production with Vincia and Pythia*, *SciPost Phys.* **12** (2022) 010, [2106.10987].

[57] ATLAS collaboration, *Measurement of the properties of Higgs boson production at $\sqrt{s} = 13$ TeV in the $H \to \gamma\gamma$ channel using 139 fb^{-1} of pp collision data with the ATLAS experiment*, 2207.00348.

[58] ATLAS collaboration, *Measurements of Higgs boson production by gluon−gluon fusion and vector-boson fusion using $H \to WW^* \to e\nu\mu\nu$ decays in pp collisions at $\sqrt{s} = 13$ TeV with the ATLAS detector*, 2207.00338.

[59] ATLAS collaboration, G. Aad et al., *Higgs boson production cross-section measurements and their EFT interpretation in the 4ℓ decay channel at $\sqrt{s}$ =13 TeV with the ATLAS detector*, *Eur. Phys. J. C* **80** (2020) 957, [2004.03447].

[60] CMS collaboration, A. M. Sirunyan et al., *Measurements of Higgs boson production cross sections and couplings in the diphoton decay channel at $\sqrt{s}$ = 13 TeV*, *JHEP* **07** (2021) 027, [2103.06956].

[61] CMS collaboration, *Measurements of the Higgs boson production cross section and couplings in the W boson pair decay channel in proton-proton collisions at $\sqrt{s}$ = 13 TeV*, 2206.09466.

[62] A. Buckley et al., *A comparative study of Higgs boson production from vector-boson fusion*, *JHEP* **11** (2021) 108, [2105.11399].

[63] T. Han, G. Valencia and S. Willenbrock, *Structure function approach to vector boson scattering in p p collisions*, *Phys. Rev. Lett.* **69** (1992) 3274–3277, [hep-ph/9206246].

[64] P. Bolzoni, F. Maltoni, S.-O. Moch and M. Zaro, *Higgs production via vector-boson fusion at NNLO in QCD*, *Phys. Rev. Lett.* **105** (2010) 011801, [1003.4451].

[65] P. Bolzoni, F. Maltoni, S.-O. Moch and M. Zaro, *Vector boson fusion at NNLO in QCD: SM Higgs and beyond*, *Phys. Rev. D* **85** (2012) 035002, [1109.3717].

[66] T. Liu, K. Melnikov and A. A. Penin, *Nonfactorizable QCD Effects in Higgs Boson Production via Vector Boson Fusion*, *Phys. Rev. Lett.* **123** (2019) 122002, [1906.10899].

[67] F. A. Dreyer, A. Karlberg and L. Tancredi, *On the impact of non-factorisable corrections in VBF single and double Higgs production*, *JHEP* **10** (2020) 131, [2005.11334].

[68] B. R. Webber, *Factorization and jet clustering algorithms for deep inelastic scattering*, *J. Phys. G* **19** (1993) 1567–1575.

[69] S. Catani, B. R. Webber and G. Marchesini, *QCD coherent branching and semiinclusive processes at large x*, *Nucl. Phys.* **B349** (1991) 635–654.

[70] S. Catani and M. H. Seymour, *A General algorithm for calculating jet cross-sections in NLO QCD*, *Nucl. Phys.* **B485** (1997) 291–419, [hep-ph/9605323].

[71] M. Ritzmann, D. A. Kosower and P. Skands, *Antenna Showers with Hadronic Initial States*, *Phys. Lett. B* **718** (2013) 1345–1350, [1210.6345].

[72] S. Ferrario Ravasio, K. Hamilton, A. Karlberg, G. P. Salam, L. Scyboz and G. Soyez, *A parton shower with higher-logarithmic accuracy for soft emissions*, 2307.11142.

[73] V. Antonelli, M. Dasgupta and G. P. Salam, *Resummation of thrust distributions in DIS*, *JHEP* **02** (2000) 001, [hep-ph/9912488].

[74] K. Hamilton, A. Karlberg, G. P. Salam, L. Scyboz and R. Verheyen, *Matching and event-shape NNDL accuracy in parton showers*, *JHEP* **03** (2023) 224, [2301.09645].

[75] J. Cruz-Martinez, T. Gehrmann, E. W. N. Glover and A. Huss, *Second-order QCD effects in Higgs boson production through vector boson fusion*, *Phys. Lett. B* **781** (2018) 672–677, [1802.02445].

[76] F. A. Dreyer and A. Karlberg, *Fully differential Vector-Boson Fusion Higgs Pair Production at Next-to-Next-to-Leading Order*, *Phys. Rev. D* **99** (2019) 074028, [1811.07918].

[77] K. Asteriadis, F. Caola, K. Melnikov and R. Röntsch, *NNLO QCD corrections to weak boson fusion Higgs boson production in the $H \to b\bar{b}$ and $H \to WW^* \to 4l$ decay channels*, *JHEP* **02** (2022) 046, [2110.02818].

[78] B. Andersson, G. Gustafson, L. Lonnblad and U. Pettersson, *Coherence Effects in Deep Inelastic Scattering*, *Z. Phys.* **C43** (1989) 625.

[79] K. Hamilton, R. Medves, G. P. Salam, L. Scyboz and G. Soyez, *Colour and logarithmic accuracy in final-state parton showers*, *JHEP* **03** (2021) 041, [2011.10054].

[80] V. N. Gribov and L. N. Lipatov, *Deep inelastic e p scattering in perturbation theory*, *Sov. J. Nucl. Phys.* **15** (1972) 438–450.

[81] Y. L. Dokshitzer, *Calculation of the Structure Functions for Deep Inelastic Scattering and e+ e- Annihilation by Perturbation Theory in Quantum Chromodynamics.*, *Sov. Phys. JETP* **46** (1977) 641–653.

[82] G. Altarelli and G. Parisi, *Asymptotic Freedom in Parton Language*, *Nucl. Phys.* **B126** (1977) 298–318.

[83] G. P. Salam and J. Rojo, *A Higher Order Perturbative Parton Evolution Toolkit (HOPPET)*, *Comput. Phys. Commun.* **180** (2009) 120–156, [0804.3755].

[84] S. Catani, Y. L. Dokshitzer, F. Fiorani and B. R. Webber, *Average number of jets in e+ e- annihilation*, *Nucl. Phys.* **B377** (1992) 445–460.

[85] S. Catani, Y. L. Dokshitzer and B. R. Webber, *Average number of jets in deep inelastic scattering*, *Phys. Lett. B* **322** (1994) 263–269.

[86] R. Medves, A. Soto-Ontoso and G. Soyez, *Lund and Cambridge multiplicities for precision physics*, *JHEP* **10** (2022) 156, [2205.02861].

[87] A. Banfi, G. P. Salam and G. Zanderighi, *Principles of general final-state resummation and automated implementation*, *JHEP* **03** (2005) 073, [hep-ph/0407286].

[88] S. Catani and M. Grazzini, *An NNLO subtraction formalism in hadron collisions and its application to Higgs boson production at the LHC*, *Phys. Rev. Lett.* **98** (2007) 222002, [hep-ph/0703012].

[89] I. W. Stewart, F. J. Tackmann and W. J. Waalewijn, *N-Jettiness: An Inclusive Event Shape to Veto Jets*, *Phys. Rev. Lett.* **105** (2010) 092002, [1004.2489].

[90] M. Dasgupta and G. P. Salam, *Resummation of the jet broadening in DIS*, *Eur. Phys. J. C* **24** (2002) 213–236, [hep-ph/0110213].

[91] M. Dasgupta and G. P. Salam, *Resummed event shape variables in DIS*, *JHEP* **08** (2002) 032, [hep-ph/0208073].

[92] M. Dasgupta and Y. Delenda, *The Q(t) distribution of the Breit current hemisphere in DIS as a probe of small-x broadening effects*, *JHEP* **08** (2006) 080, [hep-ph/0606285].

[93] M. Dasgupta and G. Salam, *Resummation of nonglobal QCD observables*, *Phys. Lett. B* **512** (2001) 323–330, [hep-ph/0104277].

[94] M. Dasgupta and G. P. Salam, *Accounting for coherence in interjet E(t) flow: A Case study*, *JHEP* **03** (2002) 017, [hep-ph/0203009].

[95] S. Caletti, O. Fedkevych, S. Marzani, D. Reichelt, S. Schumann, G. Soyez et al., *Jet angularities in Z+jet production at the LHC*, *JHEP* **07** (2021) 076, [2104.06920].

[96] ATLAS collaboration, G. Aad et al., *Search for the $HH \to b\bar{b}b\bar{b}$ process via vector-boson fusion production using proton-proton collisions at $\sqrt{s} = 13$ TeV with the ATLAS detector*, *JHEP* **07** (2020) 108, [2001.05178].

[97] NNPDF collaboration, R. D. Ball et al., *The path to proton structure at 1% accuracy*, *Eur. Phys. J. C* **82** (2022) 428, [2109.02653].

[98] A. Buckley, J. Ferrando, S. Lloyd, K. Nordström, B. Page, M. Rüfenacht et al., *LHAPDF6: parton density access in the LHC precision era*, *Eur. Phys. J. C* **75** (2015) 132, [1412.7420].

[99] S. Mrenna and P. Skands, *Automated Parton-Shower Variations in Pythia 8*, *Phys. Rev. D* **94** (2016) 074005, [`1605.08352`].

[100] M. Cacciari, G. P. Salam and G. Soyez, *The anti-k_t jet clustering algorithm*, *JHEP* **04** (2008) 063, [`0802.1189`].

[101] M. Cacciari, G. P. Salam and G. Soyez, *FastJet User Manual*, *Eur. Phys. J.* **C72** (2012) 1896, [`1111.6097`].

[102] Y. L. Dokshitzer, G. D. Leder, S. Moretti and B. R. Webber, *Better jet clustering algorithms*, *JHEP* **08** (1997) 001, [`hep-ph/9707323`].

[103] M. Wobisch and T. Wengler, *Hadronization corrections to jet cross-sections in deep inelastic scattering*, in *Workshop on Monte Carlo Generators for HERA Physics (Plenary Starting Meeting)*, pp. 270–279, 4, 1998. `hep-ph/9907280`.

[104] J. C. Collins, *Spin Correlations in Monte Carlo Event Generators*, *Nucl. Phys.* **B304** (1988) 794–804.

[105] I. Knowles, *Angular Correlations in QCD*, *Nucl. Phys. B* **304** (1988) 767–793.

[106] I. Knowles, *Spin Correlations in Parton - Parton Scattering*, *Nucl. Phys. B* **310** (1988) 571–588.

[107] I. G. Knowles, *A Linear Algorithm for Calculating Spin Correlations in Hadronic Collisions*, *Comput. Phys. Commun.* **58** (1990) 271–284.

[108] A. Karlberg, G. P. Salam, L. Scyboz and R. Verheyen, *Spin correlations in final-state parton showers and jet observables*, *Eur. Phys. J. C* **81** (2021) 681, [`2103.16526`].

[109] K. Hamilton, A. Karlberg, G. P. Salam, L. Scyboz and R. Verheyen, *Soft spin correlations in final-state parton showers*, *JHEP* **03** (2022) 193, [`2111.01161`].